An Energy Balance Model for Paleoclimate Transitions

Brady Dortmans, William F. Langford, and Allan R. Willms

Department of Mathematics and Statistics, University of Guelph, 50 Stone Road West, Guelph, ON, Canada N1G 2W1

Correspondence to: W. F. Langford (wlangfor@uoguelph.ca)

Abstract. A new energy balance model (EBM) is presented and is used to study Paleoclimate transitions. While most previous EBMs dealt only with the globally averaged climate, this new EBM has three variants: Arctic, Antarctic and Tropical climates. This EBM incorporates the greenhouse warming effects of both carbon dioxide and water vapour, and also includes ice-albedo feedback. The main conclusion to be drawn from the EBM is that the climate system possesses multiple equilibrium states, both warm and frozen, which coexist mathematically. While the actual climate can exist in only one of these states at any given time, the climate can undergo transitions between the states, via mathematical saddlenode bifurcations. This paper proposes that such bifurcations have actually occurred in Paleoclimate transitions. The EBM is applied to the study of the *Pliocene Paradox*, the *Glaciation of Antarctica* and the so-called *warm, equable climate problem* of both the mid-Cretaceous Period and the Eocene Epoch. In all cases, the EBM is in qualitative agreement with the geological record.

1 Introduction

For most of the paleoclimate history of the Earth, the climate of both polar regions was mild and free of permanent ice-caps. Today, both North and South Poles are ice-capped; however, there is overwhelming evidence that these polar ice-caps are now melting. The Arctic is warming faster than any other region on Earth. The formation of the present-day Arctic and Antarctic ice-caps occurred at widely separated times in the geological history of the Earth. This paper explores the underlying mechanisms and forcing factors that have caused climate transitions in the past. The knowledge gained here will be applied in a subsequent paper to the important problem of forecasting anthropogenic climate change.

We present a new two-layer energy balance model (EBM) for the climate of the Earth. The understanding of climate and of climate change has been advanced by many studies employing EBMs: (Budyko (1968); Dortmans et al. (2017); Kaper and Engler (2013); McGeehee and Lehman (2012); North et al. (1981); Payne et al. (2015); Sagan and Mullen (1972); Sellers (1969)). In general, these simple EBMs facilitate exploration of the relationship between specific climate forcing mechanisms and the resulting climate changes. The EBM presented here includes a more accurate representation of the role of greenhouse gases in climate change than has been the case for previous EBM's. The model is based on fundamental principles of atmospheric physics, such as the Beer-Lambert Law, the Stefan-Boltzmann Law, the Clausius-Clapeyron equation and the ideal gas equa-

tion. In particular, the modelling of water vapour acting as a greenhouse gas in the atmosphere, presented in Subsection 2.3.3, is more physically accurate that in previous EBMs and it leads to new insights for climate change.

During the early Pliocene Epoch, 3–5 Ma, the climate of the Arctic region of Earth changed abruptly from ice-free to ice-capped. The climate forcing factors then (solar constant, orbital parameters, CO_2 concentration and locations of the continents)

5 were all very similar to today. Therefore, it is difficult to explain why the early Pliocene climate was so different from that of today. That problem is known as the *Pliocene Paradox*, (Cronin (2010); Fedorov et al. (2006, 2010)). This paper presents a plausible explanation of the Pliocene paradox.

In the mid-Cretaceous Period (100 Ma) the climate of the entire Earth was much more *equable* than it is today. This means that, compared to today, the pole-to-equator temperature gradient was much smaller and also the summer/winter variation in

10 temperature at mid to high latitudes was much less. The differences in forcing factors between the Cretaceous Period and modern times appear to be insufficient to explain this difference in the climates. Eric Barron called this *the warm, equable Cretaceous climate problem* and he studied this problem in a series of papers the 1980's (Barron et al. (1981); Barron (1983)). In a similar context, Huber and Caballero (2011) and Sloan and Barron (1990, 1992) have observed that the early Eocene (56–48 Ma) encompasses the warmest climates of the past 65 million years, yet climate reconstruction studies have failed to

15 reproduce such warm temperatures. Therefore, this situation has been called the *early Eocene equable climate problem*. The present paper presents a mathematical model that gives plausible solutions to both the Cretaceous and the early Eocene equable climate problems. The key to the solution is that this model, like the actual climate, is *nonlinear* and therefore may exhibit multiple solution states for the same forcing parameters.

The end of the warm equable climate at the South Pole after the Cretaceous Period, leading eventually to abrupt glaciation

20 of Antarctica about 34 Ma, is believed to have been caused by two major geological changes. One is the movement of the Continent of Antarctica from the Southern Pacific Ocean to its present position over the South Pole, followed by the creation of the Antarctic Circumpolar Current (ACC), thus drastically reducing ocean heat transport to the South Pole; see Scher et al. (2015). The second is the gradual draw-down in CO_2 concentration world-wide; see DeConto et al. (2008); Goldner, et al. (2014); Pagani et al. (2011). The EBM of this paper supports the proposition that both of these mechanisms are required to

25 explain the abrupt Antarctic glaciation.

The energy balance model presented here is conceptual. It contains many simplifying assumptions and is not intended to give a complete detailed description of the climate of the Earth. It complements, rather than replaces, more detailed General Circulation Models (GCM). This model suggests lines of further research to be carried out with a hierarchy of more sophisticated mathematical models. Such research is already under way and will be reported elsewhere.

30 As stated above, a key feature of this family of mathematical models is that they incorporate physical principles that are *nonlinear*. As is well known, nonlinear equations can have multiple solutions, unlike linear equations which can have only one unique solution (if well-posed). In our mathematical models, the same set of equations can have two or more co-existing solutions, for example an ice-capped solution (like today's climate) and an ice-free solution (like the Cretaceous climate), even with the same values of the forcing parameters. The determination of which solution is actually realized by the planet at a

35 given time is dependent on past history. Changes in forcing parameters may drive the system abruptly from one stable state

to another, at so-called "tipping points". In this paper, these tipping points are investigated mathematically, and are shown to be *bifurcation points*, which can be investigated using *mathematical bifurcation theory*. Bifurcation theory tells us that the existence of bifurcation points is preserved (but the numerical values may change) under small deformations of the model equations. Thus, even though this conceptual model may not give us precise quantitative information about climate changes,

5 qualitatively there is good reason to believe that the *existence* of the bifurcation points in the model will be preserved in similar more refined models and in the real world.

Geometrically, this model is as simple as possible. It follows in a long tradition of *slab models* of the atmosphere. Previous slab models represented the atmosphere of the Earth as a globally-averaged uniform slab at a single temperature T. The temperature T is determined in those models by a global energy balance equation of the form *energy in = energy out*. Such

10 models are unable to differentiate between different climates at different latitudes; for example, if the polar climate is changing more rapidly that the tropical climate. In this new model, the forcing parameters of the slab atmosphere are chosen to represent one of three particular latitudes: Arctic, Antarctic or Tropics. Each of these regions is represented by its own slab model, with its own forcing parameters and its own surface temperature T_S. In addition, each region has its own variable I_A representing the intensity of the radiation emitted by the atmosphere. The two independent variables I_A and T_S are determined in each model

15 by two energy balance equations, expressing energy balance in the atmosphere and energy balance at the surface, respectively. In this way, the different climate responses of these three regions to their respective forcings can be explored.

The role played by greenhouse gases in climate change is a particular focus of this model. Greenhouse gases trap heat emitted by the surface and are major contributors to global warming. The very different roles of the two principal greenhouse gases in the atmosphere, carbon dioxide and water vapour, are analyzed here in Sections 2.3.2 and 2.3.3, respectively. The greenhouse

20 warming effect of CO_2 increases with the density of the atmosphere but is independent of temperature, while the greenhouse warming of H_2O increases with temperature but is independent of the density (or partial pressure) of the other gases present. Furthermore, as an increase in CO_2 concentration causes climate warming, this warming causes an increase in evaporation of H_2O into the atmosphere, which further increases the climate warming beyond that due to CO_2 alone (this is true both in the model and in the real atmosphere). This effect is known as *water vapour feedback*. The energy balance model presented here

25 is the first EBM to incorporate these important roles of the greenhouse gases in such detail.

2 The Energy Balance Climate Model

In this energy balance model (EBM), the atmosphere and surface are each assumed to be in energy balance. The surface layer absorbs short-wave radiant energy from the sun, and re-emits long wave radiant energy of intensity I_S, upward into the atmosphere. The atmosphere is modelled as a slab, with greenhouse gases that absorb a fraction η of the radiant energy I_S

30 from the surface. The atmosphere re-emits radiant energy of total intensity I_A. Of this radiation I_A, a fraction β is directed downward to the surface, and the remaining fraction $(1 - \beta)$ goes upward and escapes to space.

This model is based on the uniform slab EBM used in Payne et al. (2015), modified as shown in Figure 1 and further modified below. In our case, the "slab" is a uniform column of air, of unit cross-section, extending vertically above the surface to the tropopause, and located either at a pole or at the equator. The symbols in Figure 1 are defined in Table 1.
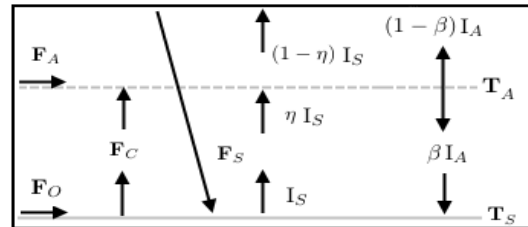
Figure 1. A visualization of the energy balance model. Symbols are defined in Table 1.

This section presents the mathematical derivation of the EBM. Readers interested only in the climate applications of the model may skip this Section and go directly to Section 3. A preliminary version of this EBM was presented in a conference proceedings paper, Dortmans et al. (2017). The present model incorporates several important improvements over that model. The differences between that model and the one presented here are indicated where appropriate in the text. Furthermore, in the previous paper, Dortmans et al. (2017) considered only the application of the model to the Arctic climate and the Pliocene Paradox; it did not study Antarctic or Tropical climate or the Cretaceous Period, as does the present paper.

In previous slab models, including Dortmans et al. (2017) and Payne et al. (2015), it was assumed that $\beta = \frac{1}{2}$; that is, the upward and downward radiation intensities from the atmosphere are made equal, see Figure 1. This would be the case for an actual uniform slab; however, the real atmosphere in not uniform in temperature nor density, and in fact both the temperature and density of the atmosphere are much higher in value near the surface than near the tropopause. The net effect of this non-uniformity is that, of the total radiation intensity I_A emitted by the atmosphere, almost two-thirds reaches the surface and only a little more than one-third escapes to space; IPCC (2013). Therefore, in order to have the model in this paper represent the atmosphere more realistically, we choose $\beta = 0.63$ instead of 0.50.

2.1 Energy Balance

The model consists of two energy balance equations, one for the atmosphere and one for the surface. In Figure 1, the so-called *forcings* are shown as arrows, pointing in the direction of energy transfer. These forcings are defined in Table 1. From Figure 1, the energy balance equations for the atmosphere and surface are given respectively by

$$0 \;=\; F_A + F_C + \eta I_S - I_A, \quad \text{and} \tag{1}$$

$$0 \;=\; F_S - F_C + F_O + \beta I_A - I_S. \tag{2}$$

Here F_C is the heat transport by conduction/convection from the surface to the atmosphere. For the Arctic model, F_C is assumed negligible; it becomes important only in the Tropics model of Section 3.3. The forcings F_O and F_A represent

Variables and Parameters Used		
Variables	**Symbol**	**Values**
Mean temperature of the surface	T_S	-50 to +20 C
Infrared radiation from the surface	I_S	141 to 419 W m^{-2}
Mean temperature of the atmosphere	T_A	-70 to 0 C
Energy emitted by the atmosphere	I_A	87 to 219 W m^{-2}
Parameters and Constants	**Symbol**	**Values**
Temperature of freezing point for water	T_R	273.15 K
Stefan-Boltzmann constant	σ	5.670 10^{-8} W m^{-2} K^{-4}
Emissivity of dry air	ϵ	0.9
Greenhouse gas absorptivity	η	0 to 1
Absorptivity for CO_2	η_C	0 to 1
Absorptivity for H_2O	η_W	0 to 1
Portion of I_A reaching surface	β	0.63
Ocean heat transport	F_O	20 to 60 W m^{-2}
Atmospheric heat transport	F_A	10–127 W m^{-2}
Heat transport by conduction / latent heat	F_C	0–100 W m^{-2}
Absorption of solar radiation	F_S	$(1-\alpha)Q$
Incident solar radiation at Poles	Q_P	173.2 W m^{-2}
Incident solar radiation at Equator	Q_E	418.8 W m^{-2}
Molar concentration of CO_2 in ppm	μ	270 to 600 ppm
Relative humidity of H_2O	δ	0 to 1
Absorption coefficient for CO_2	k_C	0.0474 m^2 kg^{-1}
Absorption coefficient for H_2O	k_W	0.0062 m^2 kg^{-1}
Warm surface albedo for ocean	α_W	0.08
Cold surface albedo for Arctic	α_C	0.7
Cold surface albedo for Antarctic	α_C	0.8
Albedo transition rate (in tanh function)	$\omega = \Omega/T_R$	0.01
Standard atmosphere lapse rate	Γ	6.49×10^{-3} K m^{-1}
Normalized standard lapse rate	$\gamma = \Gamma/T_R$	2.38×10^{-5} m^{-1}
Tropopause height at poles	Z_P	9 km
Latent heat of vaporization of water	L_v	2.2558 10^6 m^2 s^{-2}
Universal ideal gas constant	R	8.3145 kg m^2 s^{-2} K^{-1} mol^{-1}
Ideal gas constant specific to water vapour	R_W	461.4 m^2 s^{-2} K^{-1}
Saturated partial pressure of water at T_R	$P_W^{sat}(T_R)$	611.2 Pa
Saturated density of water vapour at T_R	$\rho_W^{sat}(T_R)$	4.849 10^{-3} kg m^{-3}

Table 1. Summary of variables and parameters used in the model. Antarctic surface albedo is higher than Arctic albedo because the ice/snow is purer. For details see Dortmans (2017).

ocean and atmosphere heat transport, respectively. In this model the short wave radiation from the sun F_S passes through the atmosphere without being absorbed. At the surface, the amount of solar radiation absorbed is determined by the annually averaged intensity of solar radiation striking the surface, Q, and by the *albedo* of the surface, α, which is the fraction of Q reflected by the surface back into space. Thus

$$F_S = (1 - \alpha)Q. \tag{3}$$

The value of Q at either Pole is $Q = 173.2\,\mathrm{Wm}^{-2}$ and at the Equator is $418.8\,\mathrm{Wm}^{-2}$ (McGeehee and Lehman (2012); Kaper and Engler (2013)). Typical values of the albedo α are $0.6 - 0.9$ for snow, $0.4 - 0.7$ for ice, 0.2 for cropland and 0.1 or less for open ocean.

In previous papers, including Dortmans et al. (2017), two discrete values of α are used for polar albedo: a cold albedo α_C for the ice/snow covered surface below the freezing temperature, and a warm albedo α_W corresponding to land or open ocean above the freezing temperature, that is

$$\alpha = \begin{cases} \alpha_c & \text{if } T_S \leq 273.15\,\mathrm{K}, \\ \alpha_w & \text{if } T_S > 273.15\,\mathrm{K}. \end{cases} \tag{4}$$

This discontinuous albedo function is conceptually simple but it is not an accurate representation of what would actually happen if the polar region cooled from ice-free to ice-covered. Recall that this model represents the annually averaged climate. As the polar region cools, there will be a transition period of time in which warm ice-free summers get shorter and cold ice-covered winters get longer. The annually averaged albedo, therefore, would not jump abruptly from low to high constant values as in (4); it would transition more smoothly between the summer and winter extreme values. Therefore, in this paper we introduce a more realistic (and smooth) sigmoidal albedo given by the hyperbolic tangent function as in (5); see Figure 2.

$$\alpha(T_S) = \frac{1}{2}\left([\alpha_W + \alpha_C] + [\alpha_W - \alpha_C]\tanh\left(\frac{T_S - 273.15}{\Omega}\right)\right). \tag{5}$$

The parameter Ω determines the steepness of the transition between α_W and α_C. In this paper, we use $\omega \equiv \Omega/273.15 = 0.01$.

The emission of long wave radiation from the surface is governed by the *Stefan-Boltzmann law*, that is

$$I_S = \epsilon\sigma T_S^4, \tag{6}$$

where $\sigma = 5.670 \times 10^{-8}\,\mathrm{W \cdot m^{-2} \cdot K^{-4}}$ is the Stefan-Boltzmann constant and ϵ is the emissivity, $0 < \epsilon < 1$. The surface of the Earth acts as a black-body, so $\epsilon = 1$ in (6).

Consider the atmosphere equation of the EBM, that is equation (1). Previous authors have postulated a uniform atmospheric temperature T_A for the slab model, satisfying the Stefan-Boltzmann law

$$I_A = \epsilon\sigma T_A^4, \tag{7}$$

where I_A is the intensity of radiation emitted by the atmosphere. The emissivity is $\epsilon = 0.9$ since the atmosphere is an imperfect black-body. Here, T_A is an idealized uniform atmospheric temperature, which does not exist in the real world. Previous two-layer EBMs have used (T_S, T_A) as the two independent variables in the two energy balance equations (1) and (2). However,
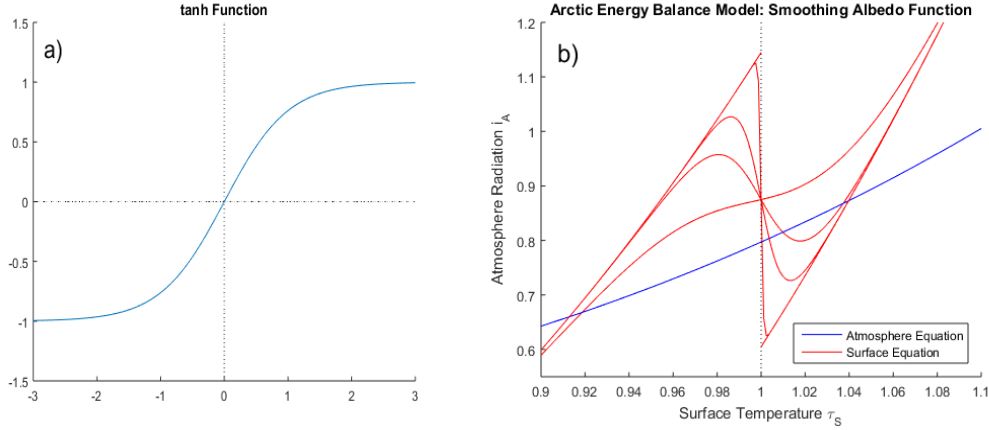
Figure 2. Subfigure a): Graph of the function tanh(x). Subfigure b): Graphs of the surface energy balance equation (12) using (4) and (5) for α, with $\alpha_c = 0.7$, $\alpha_w = 0.08$ and with $\delta = 0.0$, $\mu = 800$, $F_A = 115\,\mathrm{W m^{-2}}$ and $\omega \equiv \frac{\Omega}{T_R} = 0.001,\ 0.01,\ 0.02,\ 0.5$, in (5). There are up to 3 intersections of the blue atmosphere balance equation (11) with the red surface balance equation (12) using (5), in the figure.

the value of T_A can not be measured physically, while I_A is a real physical quantity that can be measured with some accuracy. In the present model we choose to avoid use of T_A, and instead use (T_S, I_A) as the two independent variables.

If I_A is the intensity of radiation *emitted* by the atmosphere, then in energy balance (i.e. *energy in = energy out*), the total of all energy *absorbed* by the atmosphere is also equal to I_A, see (1) or (8). Substituting (3) and (6) into the energy balance
5   equations (1) and (2) gives the following two equations for T_S and I_A.

$$0 \;=\; F_A + \eta \sigma T_S^4 - I_A \tag{8}$$
$$0 \;=\; (1-\alpha)Q + F_O + \beta I_A - \sigma T_S^4 \tag{9}$$

Here η represents the fraction of the radiation $I_S = \sigma T_S^4$ from the surface that is absorbed by the atmosphere and is called *absorptivity*. The major constituents of the atmosphere are nitrogen and oxygen and these gases do not absorb any infrared
10   radiation. The gases that do contribute to the absorptivity η are called *greenhouse gases*. Chief among these are carbon dioxide and water vapour. The contribution of these two greenhouse gases to η are analyzed in Sections 2.3.2 and 2.3.3, repectively. Although both contribute to warming of the climate, the underlying physical mechanisms of the two are very different. In general, the contribution to η of water vapour is a function of temperature.

2.1.1   Nondimensional Temperatures

15   In this paper, the temperature is near the freezing point of water, $T_R = 273.15\,°\mathrm{K}$. We rescale temperature by this reference temperature and define new nondimensional temperatures and new parameters

$$\tau_A = \frac{T_A}{T_R} \quad \tau_S = \frac{T_S}{T_R} \quad q = \frac{Q}{\sigma T_R^4} \quad f_O = \frac{F_O}{\sigma T_R^4} \quad f_A = \frac{F_A}{\sigma T_R^4} \quad i_A = \frac{I_A}{\sigma T_R^4} \quad \omega = \frac{\Omega}{T_R}. \tag{10}$$

Then the freezing temperature of water is represented by $\tau = 1$ and the atmosphere and surface energy balance equations (1)(2) or (8)(9) simplify to

$$i_A = f_A + \eta(\tau_S)\tau_S^4 \tag{11}$$

$$i_A = \frac{1}{\beta}\left[-(1-\alpha(\tau_S))q - f_O + \tau_S^4\right], \tag{12}$$

5   The range of surface temperatures T_S observed on Earth is actually quite limited; the minimum is well above $0\,\mathrm{K}$ and the maximum is well below the boiling point of water, $373.15\,\mathrm{K}$. Therefore, the nondimensional temperature τ lies in an interval around $\tau = 1$. In this paper, we assume $0.6 \le \tau \le 1.3$, which corresponds approximately to a range in more familiar Celsius degrees of $-100°\mathrm{C} \le T \le +80°\mathrm{C}$. Another reason for the upper limit on temperature is that the Clausius-Clapeyron Law used in Section 2.3.3 fails to apply at temperatures above the boiling point of water.

10   ## 2.2   Optical Depth and the Beer-Lambert Law

The goal of this section is to define the absorptivity parameter η in the EBM equation (11) (or (1) or (8)), in such a way that the greenhouse gases in the uniform slab model will absorb the same fraction η of the longwave radiation I_S from the surface as do the corresponding greenhouse gases in the nonuniform real atmosphere of the Earth. Previous energy balance models have assigned a constant value to η, often determined by climate data. In the present EBM, η is not constant but is a function

15 of other more fundamental physical quantities, such as μ, δ, k_C, k_W and T; see equations (21) and (28) below. This function is determined by classical physical laws. In this way, the present EBM adjusts automatically to changes in these physical quantities, and represents a major advance over previous EBMs.

   The Beer-Lambert Law states that when a beam of radiation (or light) enters a sample of absorbing material, the absorption of radiation at any point z is proportional to the intensity of the radiation $I(z)$ and also to the concentration or density of the

20 absorber $\rho(z)$. This bilinearity fails to hold at very high intensity of radiation or high density of absorber, neither of which is the case in the Earth's atmosphere. Whether this Law is applied to the uniform slab model or to the nonuniform real atmosphere, it yields the same differential equation

$$\frac{dI}{dz} = -k\rho(z)I(z), \tag{13}$$

where k $(m^2\,kg^{-1})$ is the absorption coefficient of the material, ρ $(kg\,m^{-3})$ is the density of the absorbing substance such as

25 CO_2, and z (m) is distance along the path. The differential equation (13) may be integrated from $z = 0$ (the surface) to $z = Z$ (the tropopause), to give

$$\frac{I_T}{I_S} = e^{-\int_0^Z k\rho(z)dz} \equiv e^{-\lambda}, \quad \text{where} \quad \lambda \equiv \int_0^Z k\rho(z)dz. \tag{14}$$

Here $I_T \equiv I(Z)$ is the intensity of radiation escaping to space at the Tropopause $z = Z$, and λ is the so-called *optical depth* of the material. Note that λ is dimensionless. For a mixture of n attenuating materials, with densities ρ_i, absorption coefficients

k_i and corresponding optical depths λ_i, the Beer-Lambert Law extends to

$$\frac{I_T}{I_S} = e^{-\Sigma_{i=1}^{n} \int_0^Z k_i \rho_i(z)dz} \equiv e^{-\Sigma_{i=1}^{n} \lambda_i}. \tag{15}$$

The absorptivity parameter $\eta = \frac{I_S - I_T}{I_S}$ in equations (1), (8), (11), represents the fraction of the outgoing radiation I_S from the surface that is absorbed by the greenhouse gases in the atmosphere (not to be confused with the absorption coefficient k).

5 It follows from the Beer-Lambert Law that η is completely determined by the corresponding optical depth parameter λ; that is

$$(1 - \eta) = \frac{I_T}{I_S} = e^{-\lambda} \quad \text{or} \quad \eta = 1 - e^{-\lambda}. \tag{16}$$

Equation (16) is the key to solving the problem posed in the first sentence of this subsection. For the ith absorbing gas in the slab model, we set its optical depth λ_i to be equal to the value of the optical depth that this gas has in the Earth's atmosphere as given by (14), and then combine them using (15). This calculation is presented for the case of CO_2 in subsection 2.3.2 and

10 for water vapour in 2.3.3.

2.3 Greenhouse Gases

The two principal greenhouse gases are carbon dioxide CO_2 and water vapour H_2O. Because they act in different ways, we determine the absorptivities η_C, η_W and optical depths λ_C, λ_W of CO_2 and H_2O separately, and then combine their effects using the Beer-Lambert Law for mixtures,

15 $$\eta = 1 - (1 - \eta_C)(1 - \eta_W) = 1 - e^{-\lambda_C - \lambda_W}, \tag{17}$$

as follows from equation (15). Other greenhouse gases have only minor influence and are ignored in this paper.

2.3.1 The Grey Gas Approximation

Although it is well-known that gases like CO_2 and H_2O absorb infrared radiation I_S only at specific wavelengths (spectral lines), in this paper the *grey gas approximation* is used; that is, the absorption coefficient k_C or k_W is given as a single number

20 averaged over the infrared spectrum, see Pierrehumbert (2010). The thesis Dortmans (2017) presents a survey of values in the literature for the absorption coefficients k_C and k_W of CO_2 and H_2O, respectively, in the grey gas approximation. This work need not be repeated here. The results are shown in Table 1; $k_C = 0.0474 \, \mathrm{m^2/kg}$ and $k_W = 0.0062 \, \mathrm{m^2/kg}$ are the values used in this paper.

2.3.2 Carbon Dioxide

25 The concentration of CO_2 in the atmosphere is usually expressed as a ratio, in molar parts per million (ppm) of CO_2 to dry air, and written as μ. There is convincing evidence that μ has varied greatly in the geological history of the Earth, and has decreased slowly over the past 100 million years; however, today μ is increasing due to human activity. The value before the industrial revolution was $\mu = 270$ ppm, but today μ is slightly above 400 ppm.

Although traditionally μ is measured as a ratio of molar concentrations, in practice, both the density ρ and the absorption coefficient k are expressed in mass units of kg. Therefore, before proceeding, μ must be converted from a molar ratio to a ratio of masses in units of kg. The mass of one mole of CO_2 is approximately $mm_C = 44 \times 10^{-3}$ kg/mol. The dry atmosphere is a mixture of 78% Nitrogen, 21% Oxygen and 0.9% Argon, with molar masses of 28 g/mol, 32 g/mol and 40 g/mol, respectively.

5   Neglecting other trace gases in the atmosphere, a weighted average gives the molar mass of the dry atmosphere as $mm_A = 29 \times 10^{-3}$ kg/mol. Therefore, the CO_2 concentration μ measured in molar ppm is converted to mass concentration in kg ppm by multiplication by the ratio $mm_C/mm_A \approx 1.52$. If $\rho_A(z)$ is the density of the atmosphere at altitude z in kg/m^3, then the mass density of CO_2 at the same altitude, with molar concentration μ ppm, is

$$\rho_C(z) = 1.52 \frac{\mu}{10^6} \rho_A(z) \quad kg/m^3. \tag{18}$$

10   It is known that CO_2 disperses rapidly throughout the Earth's atmosphere, so that its concentration μ may be assumed independent of location and altitude, IPCC (2013). As the density of the atmosphere decreases with altitude, the density of CO_2 decreases at exactly the same rate, according to (18). Substituting (18) into (14) determines the optical depth λ_C of CO_2

$$\lambda_C = 1.52 \frac{\mu}{10^6} k_C \int_0^Z \rho_A(z) dz. \tag{19}$$

Now consider a vertical column of air, of unit cross-section, from surface to tropopause. The integral in (19) is precisely

15   the total mass of this column, $M_A = \int_0^Z \rho_A(z) dz$ (measured in kg, since ρ_A is mass density). This total column mass can be estimated in two independent ways. First, consider the atmospheric pressure at the surface, $P_A(0) = 1.013 \times 10^5$ Pa. This is the total weight of the column in (19). Therefore, its total mass is $M_A = P_A(0)/g = 1.033 \times 10^4$, where $g = 9.81$ ms^{-2} is acceleration due to gravity. A second determination of the mass M_A of the column of air is as follows. Let $\bar{M} = 5.25 \times 10^{18}$ kg be the total mass of the atmosphere of the Earth and let $\bar{S} = 4\pi R_E^2 = 5.1 \times 10^{14}$ m^2 be the total surface area of the Earth,

20   with radius $R_E = 6.37 \times 10^6$ m. Then the mass of the unit column of atmosphere under consideration here is the mass per unit area; that is, $M_A = \bar{M}/\bar{S} = 1.03 \times 10^4$. These two calculations of M_A agree, up to the second decimal place. Therefore, the optical depth λ_C of CO_2 in the actual atmosphere in (19) is

$$\lambda_C = 1.52 \frac{\mu}{10^6} k_C M_A \approx \mu \cdot 7.44 \times 10^{-4}, \tag{20}$$

where we have used $k_C = 0.0474$ from Subsection 2.3.1. In the slab model, λ_C is chosen to have the same value as for the real

25   atmosphere in (20). With λ_C so determined, it follows from (16) that

$$\eta_C = 1 - e^{-\lambda_C} = 1 - e^{-\mu \cdot 7.44 \times 10^{-4}} \equiv 1 - \exp(-\mu \cdot G_C), \tag{21}$$

where $G_C \equiv 7.44 \times 10^{-4}$ is the greenhouse gas parameter for CO_2, as determined from (20). Substituting into the EBM equations (11)(12) yields

$$i_A = f_A + [1 - \exp(-\mu G_C)] \cdot \tau_S^4, \tag{22}$$

30   $$i_A = \frac{1}{\beta} \left(\tau_S^4 - [1 - \alpha(\tau_S)]q - f_O \right). \tag{23}$$

We call this the *dry atmosphere EBM*, because in this case there is no water vapour in the model ($\delta = 0$). It is clear that the atmosphere equilibrium equation (22) has a positive y-intercept ($i_A = f_A > 0$ at $\tau_S = 0$), while the surface equation (23) has a negative y-intercept ($i_A < 0$ at $\tau_S = 0$). Furthermore, the slope ($\frac{di_A}{d\tau_S}$) of (22) is positive but much less than that of (23). Therefore, one expects at least one point of intersection of (22) and (23) with positive (τ_S, i_A). However, because of the nonlinearity of the ice-albedo term $\alpha(\tau_S)$, there can be in fact up to 3 points of intersection, as shown in Figure 3 a). If the CO_2 level μ decreases sufficiently the warm state ($\tau_S > 1$) disappears, while as CO_2 inceases the frozen state ($\tau_S < 1$) may disappear. The CO_2 level μ is quite elevated here, because the effect of water vapour as a greenhouse gas has been ignored.
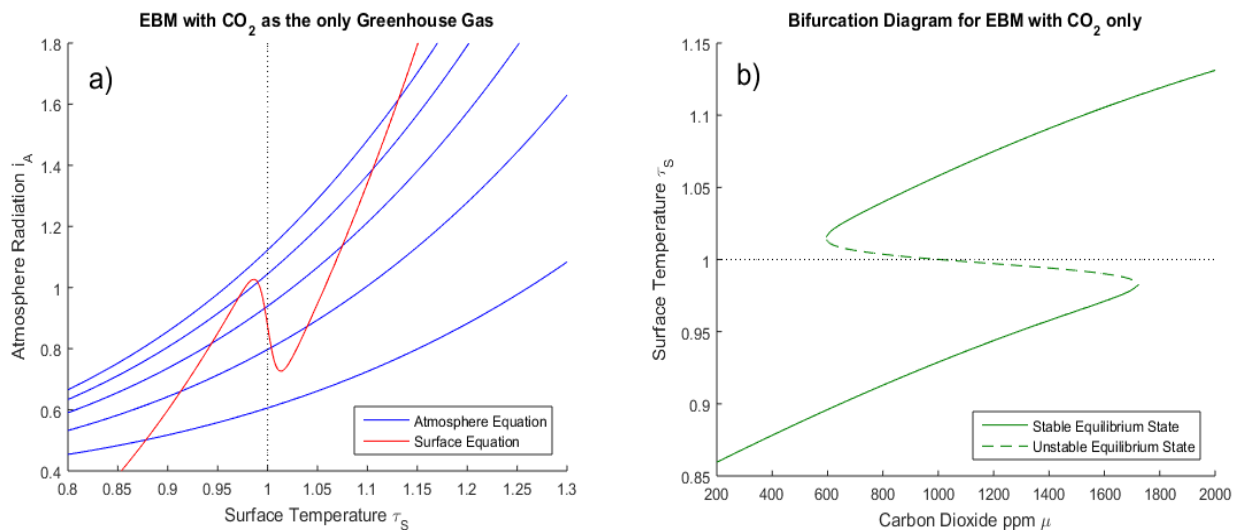
Figure 3. Dry atmosphere EBM (22)(23) (with $\delta = 0$, $F_A = 115\mathrm{Wm}^{-2}$, $F_O = 36\mathrm{Wm}^{-2}$). Subfigure a): CO_2 values $\mu = 2000, 1600, 1200, 800, 400$; from top to bottom blue curves. A unique cold equilibrium exists for $\mu = 400$, multiple equilibria exist for $\mu = 800, 1200, 1600$, and a unique warm equilibrium exists for $\mu = 2000$. Subfigure b): Bifurcation diagram for the same parameters as in a), showing the result of solving the EBM for τ_S as a function of the forcing parameter μ, holding all other forcing parameters constant. Two saddlenode (or fold) bifurcations occur, at approximately $\mu = 600$ and $\mu = 1700$. Three distinct solutions exist between these two values of μ. As μ decreases across this figure, if the surface temperature starts in the warms state ($\tau_S > 1$) then it abruptly "falls" from the warm state to the frozen state when the left bifurcation point is reached. Similarly, starting on the frozen state ($\tau_S < 1$), if μ increases sufficiently, then the state will jump upward to the warm branch when the right bifurcation point is reached. Both of these transitions are irreversible (one-way).

Figure 3 b) introduces a *bifurcation diagram* (Kuznetsov (2004)), in which the 2 EBM equations (22)(23) have been solved for the surface temperature τ_S, which is then plotted as a function of the parameter μ. Figure 3 b) shows the 3 distinct solutions τ_S of the EBM: a warm solution ($\tau_S > 1$), a frozen solution ($\tau_S < 1$), and a third solution that crosses through $\tau_S = 1$ and connects the other two solutions in *saddlenode bifurcations* (Kuznetsov (2004)). Stability analysis (Dortmans (2017)) shows that the warm and frozen solutions are *stable* (in a dynamical systems sense), while the third solution (denoted by a dashed line) is unstable.

2.3.3 Water vapour and the Clausius-Clapeyron Equation

In this section, we determine the absorptivity of water vapour as a function of temperature, $\eta_W(\tau_S)$, using fundamental physical laws including the Clausius-Clapeyron Relation, the Ideal Gas Law, and the Beer-Lambert Law, see Pierrehumbert (2010), and also assuming the idealized Lapse Rate of the International Standard Atmosphere (ISA) as defined by ICAO, see ICAO (1993).

5   Unlike CO_2, the concentration of water vapour H_2O in the atmosphere varies widely with location and altitude. This is because the partial pressure of H_2O varies strongly with the local temperature. In fact, it is bounded by a maximum saturated value, which itself is a nonlinear function of temperature, $P_W^{sat}(T)$. The actual partial pressure of water vapour is then a fraction δ of this saturated value,

$$P_W(T) = \delta\, P_W^{sat}(T), \qquad 0 \leq \delta \leq 1, \tag{24}$$

10   where δ is called *relative humidity*. While $P_W^{sat}(T)$ varies greatly with T in the atmosphere, the relative humidity δ is more nearly constant. When the actual $P_W(T)$ exceeds the saturated value $P_W^{sat}(T)$ (i.e. $\delta > 1$), the excess water vapour condenses out of the atmosphere and falls as rain or snow.

The saturated partial pressure at temperature T is determined by the *Clausius-Clapeyron equation*, see Pierrehumbert (2010),

$$15 \quad P_W^{sat}(T) = P_W^{sat}(T_R) \exp\left(\frac{L_v}{R_W} \left[\frac{1}{T_R} - \frac{1}{T} \right] \right), \tag{25}$$

where T_R is a reference temperature, here chosen to be the freezing point of water (273.15 K), L_v is the latent heat of vaporization of water and R_W is the ideal gas constant for water, see Table 1. The actual partial pressure of water vapour at relative humidity δ and temperature T is then given by combining equations (24) and (25).

We may use the *Ideal Gas Law* in the form $P_W = \rho_W R_W T$ to convert the partial pressure P_W of water vapour at temperature
20   T to mass density ρ_W of water vapour at that temperature. Substituting into (24) and (25) gives

$$\rho_W(T) = \delta \rho_W^{sat}(T) = \delta \frac{T_R}{T} \rho_W^{sat}(T_R) \exp\left(\frac{L_v}{R_W} \left[\frac{1}{T_R} - \frac{1}{T} \right] \right). \tag{26}$$

Transforming to the dimensionless temperature $\tau = T/T_R$ as in Subsection 2.1.1, this becomes

$$\rho_W(\tau) = \delta \rho_W^{sat}(\tau) = \delta \rho_W^{sat}(1) \frac{1}{\tau} \exp\left(\frac{L_v}{R_W T_R} \left[\frac{\tau - 1}{\tau} \right] \right). \tag{27}$$

The Beer-Lambert Law in Section 2.2 implies that the absorptivity of a greenhouse gas η_i is completely determined by its
25   optical depth λ_i. For water vapour, from equations (16) and (14),

$$\eta_W = 1 - e^{-\lambda_W} \qquad \text{where} \qquad \lambda_W \equiv \int_0^Z k_W \rho_W(z) dz. \tag{28}$$

Here k_W is the absorption coefficient of water vapour. In order to evaluate the integral in (28), we need to know how ρ_W varies with height z. We have shown that ρ_W is a function of temperature, given by (26) or (27). Therefore, we need an expression

for the variation of temperature T with height z. Under normal conditions, the temperature T decreases with height in the troposphere. This rate of decrease is called the *lapse rate* Γ, and defined as

$$\Gamma \equiv -\frac{dT}{dz}. \tag{29}$$

Normally, Γ is positive and is close to constant in value from the surface to the tropopause. The International Civil Aviation

5   Organization has defined, for reference purposes, the *International Standard Atmosphere* (ISA), in which Γ is assigned the constant value $\Gamma = 6.49 \times 10^{-3}$ K/m, see ICAO (1993). Using this assumption, the variation of temperature with height is given as

$$T(z) = T_S - \Gamma z \quad \text{or} \quad \tau(z) = \tau_S - \gamma z, \tag{30}$$

where the normalized lapse rate is $\gamma = \Gamma/T_R = 2.38 \times 10^{-5} \ m^{-1}$. The tropopause height Z ranges from 8 to 11 km at the

10   poles and 16 to 18 km at the equator, based on satellite measurements; see Kishore et al. (2006). Therefore, both $T(Z)$ and $\tau(Z)$ are positive. For this paper we will take the height to be $Z_P = 9$ km at the poles and $Z_E = 17$ km at the equator.

Equation (30) may be used to change the variable of integration in equation (28), for the optical depth of water vapour, from z to τ. The result is

$$\lambda_W = k_W \int_0^Z \rho_W(\tau(z))dz = \frac{k_W}{\gamma} \int_{\tau_S - \gamma Z}^{\tau_S} \rho_W(\tau)d\tau. \tag{31}$$

15   Now substitute (27) into the integral (31) and simplify to

$$\lambda_W(\tau_S) \;=\; \delta\, G_{W2} \int_{\tau_S - \gamma Z}^{\tau_S} \frac{1}{\tau} \exp\left(G_{W1}\left[\frac{\tau - 1}{\tau}\right]\right) d\tau, \tag{32}$$

where the greenhouse gas constants G_{W1} and G_{W2} for water vapour are defined as

$$G_{W1} \equiv \frac{L_v}{R_W T_R} = 17.90 \quad \text{and} \quad G_{W2} \equiv \frac{k_W \rho_W^{sat}(1)}{\gamma} = 1.265. \tag{33}$$

Finally, using the Beer-Lambert Law, the absorptivity η_W of water vapour in equation (28) is determined by its optical depth,

20   and is now a function of the surface temperature,

$$\eta_W(\tau_S) = 1 - \exp\left[-\lambda_W(\tau_S)\right] = 1 - \exp\left[-\delta\, G_{W2} \int_{\tau_S - \gamma Z}^{\tau_S} \frac{1}{\tau} \exp\left(G_{W1}\left[\frac{\tau - 1}{\tau}\right]\right) d\tau\right]. \tag{34}$$

The definite integral in this expression is easily evaluated numerically in the process of solving the atmosphere and surface EBM equations.

Figure 4(a) shows that the function $\eta_W(\tau_S)$ in (34) increases from near 0 to near 1 as τ_S increases past 1, and it steepens

25   towards a step function as δ increases. This implies that, if the surface temperature τ_S in the surface energy balance equation (12) increases past $\tau_S = 1$, then the absorptivity of water vapour $\eta_W(\tau_S)$, acting as a greenhouse gas in equation (11), increases
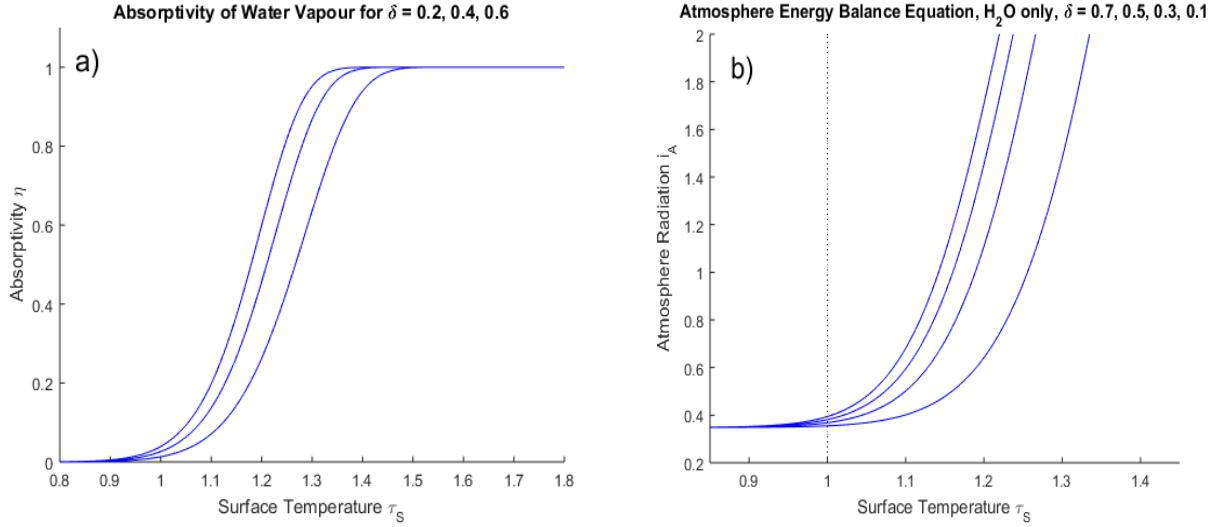
Figure 4. Greenhouse effect of Water Vapour only ($\mu = 0$). Subfigure a): Absorptivity $\eta_W(\tau_S)$ as given by equation (34) with $\delta = 0.6$, 0.4, 0.2 from top to bottom. Below freezing, $\tau_s < 1$, water vapour has very little influence as a greenhouse gas, but absorptivity increases rapidly to approach $\eta = 1$ for $\tau > 1$. Subfigure b): Atmosphere energy balance equation (36) with $\mu = 0$, and relative humidity values $\delta = 0.7$, 0.5, 0.3, 0.1, from top to bottom blue lines. There is little greenhouse effect for $\tau_S < 1$ but the greenhouse warming effect for $\tau_S > 1$ increases strongly with τ_S and with δ.

rapidly, thus amplifying the heating of the atmosphere by the radiation $I_S = \sigma T_S^4$ from the surface. Energy balance requires a corresponding increase in the radiation I_A transmitted from the atmosphere back to the surface, further increasing the surface temperature τ_S. This is a positive feedback loop called *water vapour feedback*. Figure 4 shows two views of this dramatic water vapour feedback effect. This rapid nonlinear change is due to the relatively large size of the greenhouse constant $G_{W1} =$

5 $\frac{L_v}{R_W T_R} = 17.9$, in the exponent of the Clausius-Clapeyron equation (27), as it reappears in equation (34).

2.3.4 Combined CO$_2$ and H$_2$O Greenhouse Gases

The combined effect of two greenhouse gases is determined by the Beer-Lambert Law as shown in Section 2.2. If η_C is the absorptivity of CO$_2$ as in (21) and η_W is the absorptivity of H$_2$O as in (28), then the combined absorptivity η_{CW} of the two is obtained by adding the two corresponding optical depths λ_C and λ_W,

$$\eta_{CW}(\tau_S) = 1 - \exp\left[-\lambda_C - \lambda_W(\tau_S)\right] = 1 - \exp\left[-\mu \cdot G_C - \delta\, G_{W2} \int_{\tau_S - \gamma Z}^{\tau_S} \frac{1}{\tau} \exp\left(G_{W1}\left[\frac{\tau-1}{\tau}\right]\right) d\tau\right], \quad (35)$$

After these substitutions the two-layer EBM equations (22)(23) become

$$i_A = f_A + \eta_{CW}(\tau_S) \cdot \tau_S^4, \quad (36)$$
$$i_A = \frac{1}{\beta}\left(\tau_S^4 - [1 - \alpha(\tau_S)]q - f_O\right). \quad (37)$$

where $\alpha(\tau_S)$ is defined in equation (5), $\eta_{CW}(\tau_S)$ is defined in equation (35), and the remaining parameters are given in Table 1. Note that the atmosphere radiation variable i_A is easily eliminated from equations (36)(37), leaving a single equation for the unknown equilibrium surface temperature τ_S,

$$0 = [1 - \alpha(\tau_S)]q + f_O + \beta f_A - [1 - \beta\eta_{CW}(\tau_S)]\tau_S^4. \tag{38}$$

5   This form of the EBM is useful for obtaining bifurcation diagrams.

2.4   Positive Feedback Mechanisms

The above analysis shows that there are two highly nonlinear positive feedbacks in this EBM. Consider the case of rising temperature, near the freezing point. The first feedback is due to albedo in the surface equilibrium equation. As illustrated in Figure 2, if the surface temperature increases slowly thought the freezing point, there is a large increase in energy absorbed,
10   leading to an abrupt increase in temperature. The second is water vapour feedback in the atmosphere equilibrium equation, shown in Figure 4. If the surface temperature continues to increase above freezing, then the absorptivity of water vapour increases dramatically, adding energy to the system and further increasing the temperature. Both of these forcings are called positive feedbacks, because they amplify the warming effect of the original forcing.

3   Applications of the Energy Balance Model

15   The goal of this section is an exploration of the underlying causes of abrupt climate changes that have occurred on Earth in the past 100 million years, using as a tool the EBM developed in Section 2. The most dramatic climate changes occurred in the two polar regions of the Earth. The climate of the tropical region of the Earth has changed relatively little in the past 100 million years. In mathematics, a nonlinear system can have multiple solution states coexisting at the same parameter values. A small change in the parameters may cause a solution of the system to jump from one state to another, with very different
20   characteristics. Mathematical bifurcation theory is useful for detecting and explaining such multiple states and transitions.

In this Section, the EBM is applied to the glaciation of Antarctica, the Pliocene Paradox, the warm equable Cretaceous problem and the warm equable Eocene problem. For comparison, a control EBM with parameter values set to those of the Tropics shows no abrupt climate changes in the Tropical climate for the past 100 million years.

3.1   EBM for the Glaciation of Antarctica

25   Antarctica in the mid-Cretaceous Period was ice-free, and it remained so for the remainder of the Cretaceous Period and well into the Paleogene (65 – 23 Ma). In the mid-Cretaceous, the continent of Antarctica was in the South Pacific Ocean. At that time, the South Pole was located in open ocean and was warmed by Pacific Ocean currents, as was Antarctica. However, the continent of Antarctica moved poleward and began to encroach upon the South Pole towards the end of the Cretaceous, fully covering the South Pole by the end of the Eocene, see Briggs (1987). The diminishing marine influence on the South Pole coincided
30   with the onset of cooling of Antarctica about 45 Ma (mid-Eocene). The opening of the both the Drake Passage (between South

America and Antarctica) and of the Tasmanian Gateway (between Antarctica and Australia) near the end of the Eocene (34 Ma), led to the creation of the Antarctic Circumpolar Current (ACC), which further isolated the South Pole from warm ocean heat transport and accelerated the cooling and glaciation of Antarctica; Cronin (2010). Therefore, from the early Eocene to the late Oligocene, the ocean heat transport to the South Polar region decreased significantly, from near the Cretaceous value, about

5    $100 \, \mathrm{Wm}^2$ (Barron et al. (1981)), to a much lower value, taken here to be $30 \, \mathrm{Wm}^2$. The geological record shows an abrupt drop in temperature and the onset of massive glaciation in Antarctica, at the Eocene-Oligocene boundary, about 34 MYa.

Because the atmosphere is well mixed, at any given time the CO_2 level in the Antarctic is the same as worldwide. Estimates of Eocene CO_2 concentration μ vary widely. For example Pagani et al. (2005, 2006) estimate Eocene CO_2 concentration at 1000-1500 ppm, while Wolfe et al. (2017) estimate 490 ppm. For this EBM, we estimate early Eocene global CO_2 level as

10   $\nu = 1100$ ppm. According to Pagani et al. (2005, 2006); Cronin (2010); this had decreased to approximately modern levels by the end of the Oligocene, 23 Ma, that is to $\mu = 400$ ppm.

In the recent literature, there has been a vigorous discussion of whether the primary cause of the onset of Antarctic glaciation is the slow decline in CO_2 concentration, or the decrease in poleward ocean heat transport due to the opening of ocean gateways and the creation of the ACC; see DeConto et al. (2008); Goldner, et al. (2014); Pagani et al. (2011); Scher et al. (2015). In the

15   work of Scher et al. (2015), it is observed that onset of the ACC coincided with major changes in global ocean circulation, which probably contributed to the drawdown in CO_2 concentration in the atmosphere. Since both CO_2 concentration and ocean heat transport F_O are explicit parameters in the EBM presented here, they can be varied independently in the model to investigate which one played a primary role.
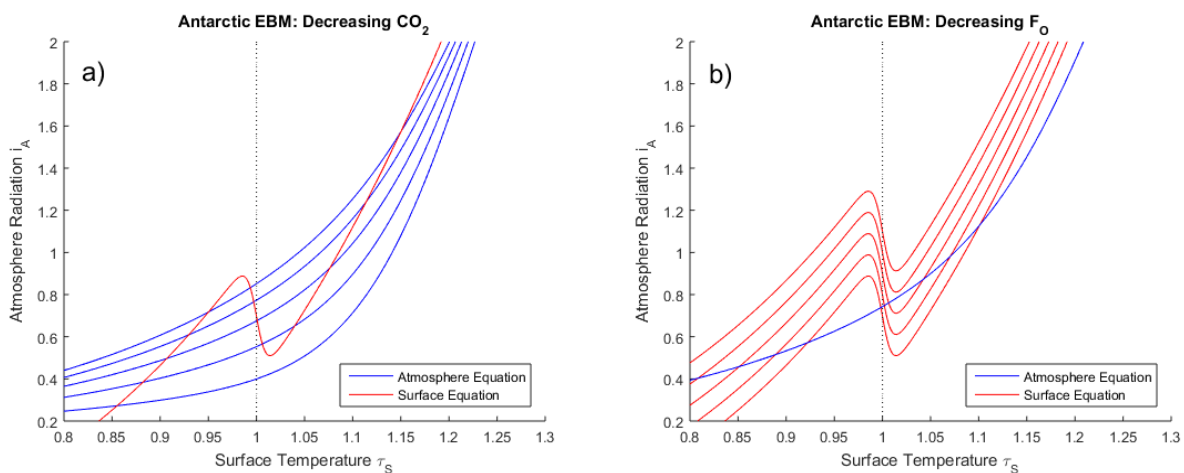
Figure 5. EBM for the Glaciation of Antarctica. Subfigure a): Graphs of EBM equations, with F_O fixed at $80 \, \mathrm{Wm}^{-2}$ in the surface equation (red line), and with CO_2 concentration μ in the atmosphere equation decreasing (from top to bottom blue lines) $\mu = 1500, 1200, 900, 600, 300$ ppm. Subfigure b): Graphs of the same EBM equations, but with CO_2 concentration μ fixed at 1100 ppm (blue line) and with ocean heat transport F_O decreasing (from bottom to top red lines) $80, 60, 40, 20, 0 \, \mathrm{Wm}^{-2}$.

Figure 5 shows the solutions of the EBM equations for Antarctic parameter values, including $F_A = 52 \text{ Wm}^{-2}$. Points of intersection of one red line (surface equation) and one blue line (atmosphere equation) are the equilibrium solutions of the system. In general, there can be up to three solutions: a frozen solution (with $\tau_S < 1$), a warm solution (with $\tau_S > 1$), and an intermediate solution, on the downward sloping portion of the red line, which is unstable in the dynamical systems sense. (The other two solutions are always stable, see Dortmans (2017).) In Figure 5 a) the ocean heat transport F_O in held fixed, while CO_2 concentration μ is decreased, from the top to bottom blue lines. In Figure 5 b) the reverse is true; the CO_2 concentration μ is held fixed while the ocean heat transport F_O is decreased, from bottom to top red lines. In each case, for a sufficiently small value of μ or F_O, respectively, the warm solution disappears. This occurs when the warm solution meets the unstable intermediate solution. When the two meet, they coalesce then disappear, in what is called a *saddlenode bifurcation* in dynamical systems theory (Kuznetsov (2004)). Beyond this bifurcation, only the frozen solution ($\tau_S < 1$) exists.

Figure 6 displays *bifurcation diagrams*, in which the surface temperature τ_S, which has been determined as a solution of the EBM, is plotted while parameters in the EBM are varied smoothly, from the early Eocene values, 55 million years ago, to the late Oligocene values, 23 million years ago. These dates are chosen to bracket the time of the glaciation of Antarctica. First we introduce a *bifurcation parameter ν*, which acts as a surrogate time variable. The bifurcation parameter ν is related to geological time by

$$t = 55 - 32 \cdot \nu \quad \text{Ma}. \tag{39}$$

Thus, $\nu = 0$ corresponds to the early Eocene 55 Ma and $\nu = 1$ corresponds to the late Oligocene 23 Ma. During this time, it is known that both CO_2 concentration μ and ocean heat transport F_O were decreasing slowly. To study the effects of the simultaneous reduction of μ and F_O, we express both as simple linear functions of the bifurcation parameter ν, as follows:

$$\mu = 1100 - 700 \cdot \nu, \tag{40}$$

$$F_O = 100 - 70 \cdot \nu, \qquad 0 \le \nu \le 1.$$

Here, $\nu = 0$ corresponds to the high early Eocene values of $\mu = 1100$ and $F_O = 100$, while $\nu = 1$ corresponds to the low Oligocene-Miocene boundary values of $\mu = 400$ and $F_O = 30$. Thus, in equations (40), as ν increases from 0 to 1, the climate forcing factors μ and F_O decrease linearly from their Eocene values to late Oligocene values. Strictly speaking, these forcings did not change linearly in time; however, the decease is fairly close to linear, and for qualitative results we can make this simplifying assumption in the EBM. The parameter F_A is held constant at $F_A = 52$, from Barron et al. (1981). Albedo for the fresh snow in Antarctica is $\alpha_C = 0.8$. Other parameters are as in Table 1.

Figure 6 a) shows a saddlenode bifurcation at $\nu = 0.606$, corresponding to forcing parameter values $\mu = 676$ ppm and $F_O = 57.6 \text{ Wm}^{-2}$ in the model, and to geological time about 35 Ma, assuming the linear time relation in (39). This corresponds remarkably closely to best estimates of the timing of glaciation in the geological record of about 34 Ma. The warm state and frozen state temperatures coexisting at the bifurcation point are $+4.6°\text{C}$ and $-40.2°\text{C}$. These temperatures are close to paleoclimate estimates (Cronin (2010)). As ν increases past the bifurcation point $\nu = 0.606$, the warm climate state ceases to exist, and the climate system transitions ("falls") rapidly, from the saddlenode point to the frozen state, Kuznetsov (2004). Thus the EBM reproduces the abrupt transition to the glaciation of Antarctica, which is seen in the geological record.
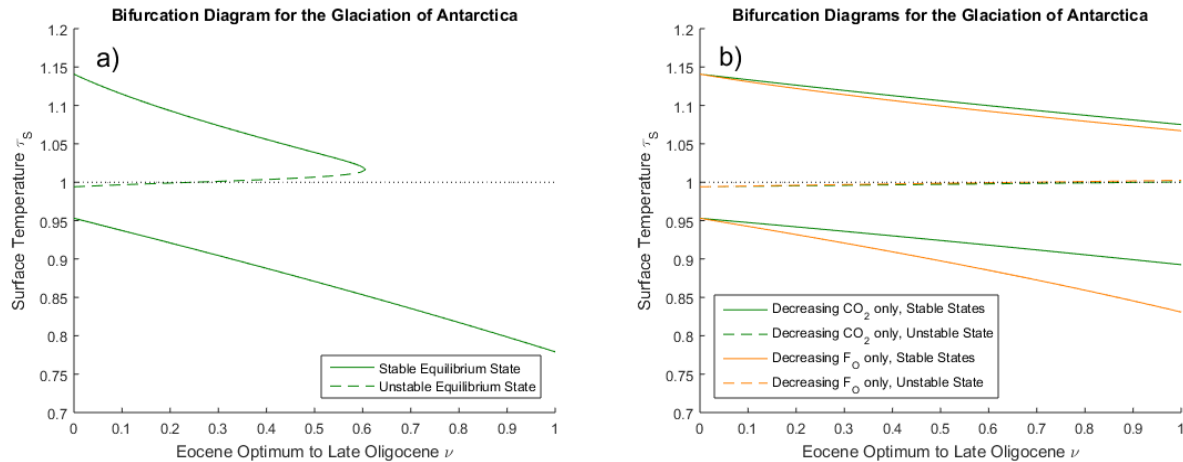
Figure 6. Bifurcation Diagrams for the Glaciation of Antarctica. Subfigure a): This shows a saddlenode bifurcation at $\nu = 0.606$, corresponding to forcing parameter values $\mu = 676$ ppm and $F_O = 57.6\,\mathrm{Wm}^{-2}$ in equations (40). As ν increases through this saddlenode bifurcation point, the climate will transition abruptly from a warm state to a frozen state. The warm state and frozen state temperatures coexisting at the bifurcation point are $+4.6\,^\circ\mathrm{C}$ and $-40.2\,^\circ\mathrm{C}$. The bifurcation point corresponds to a geological time of about 35 Ma, assuming the linear model equations (39)(40). Subfigure b): Two superimposed bifurcation diagrams as in a), except that, on the green curves, F_O is held fixed at its Eocene values while μ deceases as in (40), and on the yellow curves, μ is held fixed at the Eocene value while F_O decreases as in (40). No saddlenode bifurcation occurs in either scenario.

Figure 6 b) explores the relative importance of decreasing CO_2 concentration μ and decreasing ocean heat transport F_O in the glaciation of Antarctica. The green curves represent a scenario in which μ decreases as in equation (40) but F_O is held fixed at its Eocene value, and the yellow curves represent a case in which μ is held fixed at its Eocene value while F_O decreases according to (40). In neither case does a glaciation event occur. The analysis of this paper implies that significant decreases in *both* CO_2 concentration μ and ocean heat transport F_O are required to achieve a saddlenode bifurcation, and the observed transition to a frozen Antarctic state.

While the glaciation of Antarctica is an accepted fact in paleoclimate science, the suddenness of the climate change that occurred in Antarctica near the Eocene-Oligocene boundary (33.9 Ma), a time when the forcing parameters were changing slowly, has not been adequately explained. The bifurcation analysis presented here presents a simple but plausible explanation that fills this gap in the literature. Furthermore, this EBM supports the hypothesis that *both* falling CO_2 concentration μ and decreasing ocean heat transport F_O are essential to an explanation of the sudden glaciation of Antarctica.

3.2 EBM for the Pliocene Paradox

The Arctic region of the Earth's surface has had ice cover year-round for only the past few million years. For at least 100 million years prior to about 5 Ma, the Arctic had no permanent ice cover, although there could have been seasonal snow in the winter. Recently, investigators have found plant and animal remains, in particular on the farthest northern islands of the

Canadian Arctic Archipelago, which demonstrate that there once was a wet temperate rainforest there for millions of years, similar to that now present on the Pacific Northwest coast of North America; see Basinger et al. (1994); Greenwood et al. (2010); Jahren and Sternberg (2003); Struzik (2015); West et al. (2015); Wolfe et al. (2017). The change from ice-free to ice-covered in the Arctic occurred abruptly, during the Pliocene Epoch, 5.3 to 2.6 Ma. It has been a longstanding challenge for
5   paleoclimatologists to explain this dramatic change in the climate.

During the Pliocene Epoch, all of the important forcing factors that determine climate were very similar to those of today. The Earth orbital parameters, the CO_2 concentration, solar radiation intensity, position of the continents, ocean currents and atmospheric circulation all had values close to the values they have today. Yet, in the early Pliocene, 4–5 million years ago, the Arctic climate was much milder than that of today. Arctic surface temperatures were $8 - 19°C$ warmer than today and global
10   sea levels were $15 - 20$ m higher than today, and yet CO_2 levels are estimated to have been $340 - 400$ ppm, about the same as 20th Century values; see Ballantyne et al. (2010); Csank et al. (2011); Tedford and Harington (2003). As mentioned in the Introduction, the problem of explaining how such different climates could exist with such similar forcing parameter values has been called the *Pliocene Paradox* (Cronin (2010); Fedorov et al. (2006, 2010)).

Another interesting paradox concerning Polar glaciation is the fact that, although both poles have transitioned abruptly
15   from ice-free to ice-covered, they did so at very different geological times. The climate forcing conditions of Earth are highly symmetric between the two hemispheres and for most of the history of Earth the climates of the two poles have been very similar. However, there was an anomalous period of about 30 million years, from the Eocene-Oligocene boundary (34 Ma) to the early Pliocene (4 Ma), when the Antarctic was largely ice-covered but the Arctic was ice-free.

An important feature of Arctic climate in the early Pliocene, and for many millions of years earlier, was that the relative
20   humidity δ was much higher than today. The mid-Eocene climate has been described as a wet temperate rainforest (Greenwood et al. (2010)), with estimated relative humidity of 67% (Jahren and Sternberg (2003)), and these conditions prevailed with only minor fluctuations until the Pliocene. For this Arctic EBM, we choose $\delta = 0.67$. Important nonlinear physical relationships among the temperature, the water vapour pressure, the water vapour greenhouse heating effect and the relative humidity, were explored in Subsection 2.3.3 and incorporated into the EBM there.

25   During the Eocene (56 – 34 Ma), global temperatures were much higher than today, particularly in the Arctic (Greenwood et al. (2010); Wolfe et al. (2017); Huber and Caballero (2011)), with CO_2 concentration μ and ocean heat transport to the Arctic F_O also higher than today, and decreased slowly to today's values over geoloical time scales. For this EBM, we set mid-Eocene CO_2 at $\mu = 1000$ (Pagani et al. (2005)). The decrease in CO_2 concentration observed since the Eocene may be attributed to deceased volcanic activity, increased absorption and sequestration by vegetation, the oceans, continental erosion
30   and other sinks.

The changes in ocean heat transport to the Arctic are more complicated. There was a slow drop in global sea level, in large part due to the accumulation of vast amounts of water in the form of ice and snow on Antarctica. It has been estimated that the total amount of ice today in the Antarctic is equivalent to a change in sea level of about 58 m (Fretwell et al. (2013); IPCC (2013)). This drop in sea level likely reduced the flow of warm surface ocean water into the Arctic. However, other factors
35   were at play. In the Eocene, the North Atlantic Ocean did not yet exist, but the Turgai Strait existed between Europe and Asia

and connected the warm Indian Ocean to the Arctic. By the Miocene, The Turgai Strait had closed and the North Atlantic had opened between Greenland and Norway, forming a deep-water connection to the Arctic Ocean. During the Pliocene the formation of the Isthmus of Panama about 3.5 Ma cut off an equatorial current that had existed between the warm Atlantic and cooler Pacific, at least since Cretaceous times. On the Atlantic side of the Isthmus, the sea water became warmer, and became

5   more saline due to evaporation. The Gulf Stream carried this warm salty water to Western Europe. One might expect the Gulf Stream to transport more heat into the Arctic. However, some believe that the Gulf Stream actually contributed to glaciation in the Arctic, as follows (Haug et al. (2004); Bartoli et al. (2005)). Evaporation from the Gulf Stream waters contributed to rainfall across Northern Europe and Siberia, increasing the flow of fresh water in rivers emptying into the Arctic Ocean. This reduced the salinity, and hence the density, of the Arctic Ocean waters. The Gulf Stream waters in the North Atlantic, now

10   cooler, and denser due to high salinity, were forced downward by the less dense Arctic waters, and then returned southward as a deep ocean current, without having conveyed much heat to the Arctic. Meanwhile the low salinity Arctic surface water with a higher freezing temperature, began to freeze, resulting in higher albedo and accelerating Arctic glaciation. In the EBM, we summarize all of the above heat transport mechanisms by specifying a slow overall decrease in ocean heat transport to the Arctic, represented by the single forcing parameter F_O. As explained above, the net decrease in F_O is small.

15   Figure 7 a) shows graphs of the surface and atmosphere equilibrium equations for the Arctic Pliocene EBM, for varying values of μ. We do not show a figure with decreasing ocean heat transport F_O, analogous to Figure 5 b), because the decrease in F_O is relatively small in the Arctic. Again, it is clear that there may exist up to 3 points of intersection of a given atmosphere equilibrium curve (blue) with a surface equilibrium curve (red); namely, a warm equilibrium state $\tau_s > 0$, a frozen equilibrium state $\tau_S < 0$, and a third (intermediate) solution, which is always unstable (when it exists). Just as in Figure 5, as μ decreases

20   and the warm equilibrium state approaches the local minimum on the red S-curve, at the same time the unstable intermediate equilibrium state moves down the middle branch of the red S-curve. When they meet, these two equilibria coalesce then disappear, via a saddlenode bifurcation. Beyond this saddlenode bifurcation, only one equilibrium state remains, that is the stable frozen state. Dynamical systems theory tells us that following this bifurcation, the system will transition rapidly to that frozen equilibrium state. The paleoclimate record shows that both CO_2 concentration and ocean heat transport F_O were

25   trending downward for millions of years before the Pliocene. Therefore, Figure 7 a) predicts that an abrupt drop in temperature to a frozen state would be inevitable, if this trend continued far enough.

In order to explore this downward trend further, we bracket the Pliocene Epoch between the mid-Eocene Epoch (50 Ma) and the pre-industrial modern era (300 years ago), and define a surrogate time variable ν (as in Section 3.1) by

$$t \quad = \quad 50(1 - \nu) \quad \text{Ma}. \tag{41}$$

30   Then we express both μ and F_O as decreasing linear functions of ν

$$\mu \quad = \quad 1000 - 730 \cdot \nu \quad \text{ppm} \tag{42}$$

$$F_O \quad = \quad 60 - 10 \cdot \nu \quad \text{Wm}^{-2}.$$
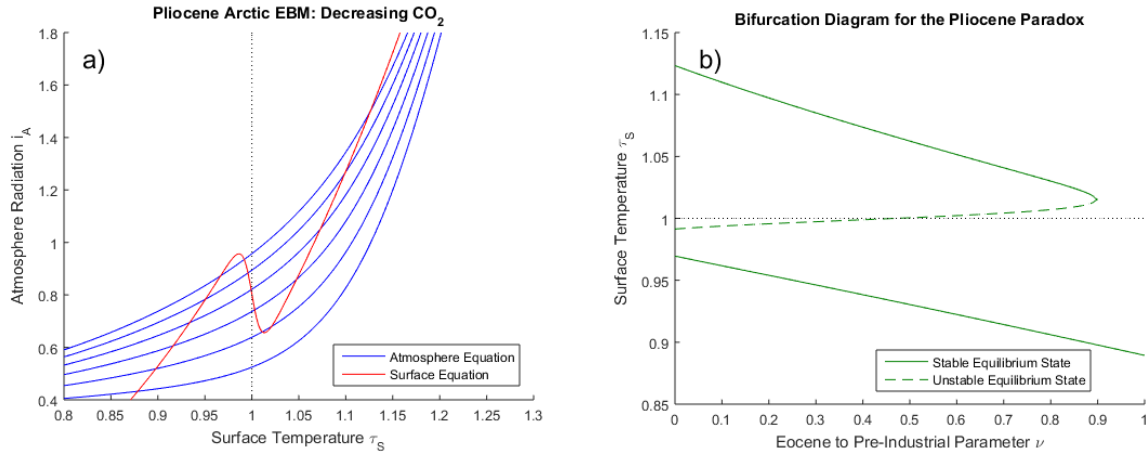
Figure 7. Pliocene Arctic EBM (36)(37). Parameter values $\delta = 0.67$, $F_A = 115$; other parameters as in Table 1. Subfigure a): CO_2 takes values $\mu = 1200, 1000, 800, 600, 400, 200$ ppm, from top to bottom on the blue curves, with fixed $F_O = 50 \, \mathrm{Wm}^{-2}$. The warm equilibrium state disappears as μ decreases. Subfigure b): Bifurcation Diagram for the Pliocene Paradox. Here, CO_2 concentration μ and ocean heat transport F_O decrease simultaneously, with increasing ν, $(0 \leq \nu \leq 1)$, as given by equations (42). As ν increases, the warm equilibrium solution ($\tau_S > 1$) disappears in a saddlenode bifurcation, at approximately $\nu = 0.9$, corresponding to forcing parameter $\mu = 343$ ppm and $F_O = 51 \, \mathrm{Wm}^2$. To the right of this point, only the frozen equilibrium state exists. To the left of this point, the frozen and warm equilibrium states coexist, separated by the unstable intermediate state.

Here, $\nu = 0$ corresponds to estimated mid-Eocene values of μ and F_O, (taken from Pagani et al. (2005); Wolfe et al. (2017); Barron et al. (1981)), while $\nu = 1$ corresponds to modern preindustrial values (IPCC (2013)). Equations (42) define μ and F_O as linear functions of ν, just as (40) did for the Antarctic model.

Figure 7 b) is a bifurcation diagram (Kuznetsov (2004)), which shows the dependence of surface temperature τ_S on this
5   bifurcation parameter ν. Note that, for $\nu = 0$ (mid-Eocene values, 50 Ma) both the warm and the frozen equilibrium states exist. However, as ν increases toward $\nu = 1$, the warm equilibrium state disappears in a saddlenode (or fold) bifurcation, leaving only the frozen equilibrium state to the right of the saddlenode bifurcation. This bifurcation occurs at approximately $\nu = 0.9$, which correspondis to $\mu = 343$ ppm and $F_O = 51 \, \mathrm{Wm}^{-2}$. The warm state and frozen state temperatures, at the bifurcation value of $\nu = 0.9$ in the EBM, are $+4.1°C$ and $-27.9°C$; reasonably close to actual Pliocene values. The surrogate
10   time of the bifurcation point, $\nu = 0.9$, corresponds to a geological time of $t = 5$ Ma, from (41), which is close to the time of glaciation of the Arctic in the geological record.

Thus, the EBM presented here, as illustrated in Figure 7, provides a plausible explanation for the Pliocene paradox. The slowly-acting physical forcings of decreasing CO_2 concentration and decreasing ocean heat transport F_O were amplified by the mechanisms of ice-albedo feedback and water vapour feedback, both of which act very strongly when the temperature crosses
15   the freezing point of water. For millions of years before the Pliocene, while the Arctic temperature remained well above freezing, the climate changed very little. However, once the freezing temperature was reached, the Arctic climate changed

abruptly via a saddlenode bifurcation as in Figure 7 b), to a new frozen state. This simple mechanism suffices to explain the Pliocene paradox. No more complicated explanations are necessary.

To summarize this section, there are in fact four different "paradoxes" associated with the Arctic climate of the Pliocene Epoch. Each of these paradoxes is resolved by the EBM of this paper, as follows.

Paradox 1: Warm equable early Pliocene climate. The early Pliocene Arctic climate was warm and equable, very different from today's climate, even though all of the forcing factors were very similar to those of today. The EBM explains that the climate system under Pliocene forcing conditions possessed two different climate states, a warm state like the early Pliocene climate and a frozen state like today's climate, coexisting mathematically for the same forcings.

Paradox 2: Mid-Pliocene abrupt climate transition. In the mid-Pliocene, the Arctic climate underwent a major and rapid excursion, from warm to frozen, even though the forcing factors were changing very slowly at the time. The EBM indicates that the climate state underwent a saddlenode bifurcation at this time, causing an abrupt transition from a warm to a frozen state.

Paradox 3: Broken North-South symmetry. The planet Earth has a remarkable North-South symmetry, with respect to all external forcing factors that determine the climate. Yet, for about 30 million years prior to the Pliocene, the Antarctic was ice-covered while the Arctic was ice-free. Decreasing carbon dioxide concentration μ caused cooling at both poles; however, μ is the same throughout the atmosphere at any given time. The EBM identifies ocean heat transport F_O as the forcing factor responsible for breaking the North-South symmetry of the planet. Due to the movement of the continental tectonic plates, ocean currents have changed significantly in the past 100 million years. For the South Pole, the effect was to reduce F_O from a very high value to a very low value; while for the North Pole, the net reduction in F_O was quite small. This more rapid cooling of Antarctica caused glaciation to occur there 30 million years before the glaciation of the Arctic.

Paradox 4: The GCM anomaly. General Circulation models (GCM), which accurately reproduce today's climate, fail to duplicate the early Pliocene warm climate when adjusted to early Pliocene forcings. The EBM suggests that these GCM simulations, starting with today's climate and moving backward in time, would have remained on the stable frozen climate state of the bifurcation diagram in Figure 7 b), and thus failed to "see" the coexisting warm state.

3.2.1 Permanent El Niño and Hadley cell feedback

Several other explanations have been proposed for the Pliocene paradox. There is convincing evidence that, at the beginning of the Pliocene, there was a permanent El Niño condition in the tropical Pacific ocean, see Cronin (2010); Fedorov et al. (2006, 2010). (However, some have disputed this finding, see Watanabe et al. (2011).) It has been suggested that a permanent El Niño condition could explain the warm early Pliocene, and that the onset of the El Niño – La Niña Southern Oscillation (ENSO) was the cause of sudden cooling of the Arctic during the Pliocene. Today, it is known that ENSO can influence weather patterns as far away as the Arctic.

Another suggestion is that Hadley cell feedback contributed to the abrupt cooling of the Arctic during the Pliocene. Recent work shows that an increase in pole-to-equator temperature gradient causes the Hadley cells to contract towards the equator, while increasing in circulation velocity, see Lewis and Langford (2008); Langford and Lewis (2009). This would cause a decrease in equator to pole atmospheric heat transport, which would in turn accelerate Arctic cooling; this is called Hadley

5   cell feedback. Further work on modelling this mechanism is in progress. It is conjectured here that Hadley cell feedback may in fact have caused the end of a permanent El Niño condition in the Pliocene, as follows. It is known that the La Niña phase of ENSO is forced in part by the Trade Winds blowing East to West across the tropical Pacific Ocean. The Trade Winds are the surface component of the Hadley circulation. Therefore, acceleration of the Hadley circulation would strengthen the Trade Winds, enhancing the conditions for La Niña and ending the permanent El Niño. Further work on this conjecture also is in

10   progress.

3.3   EBM for the Tropics

In the Tropics, many of the values of the forcing parameters are different from their values in the Arctic and Antarctic, see Table 2. The geological record shows little change in the tropical climate over the past 100 million years, other than a little cooling. Even when Arctic climate changed dramatically in the Pliocene, the Tropical climate changed very little.

Forcing Parameter Values for the Tropics EBM		
Parameter	**Modern Arctic Value**	**Tropics Value**
Relative humidity δ	0.4	0.7
Ocean heat transport F_O	20-60 Wm^{-2}	-20 Wm^{-2}
Atmospheric heat transport F_A	70-120 Wm^{-2}	-18 Wm^{-2}
Latent heat transport F_C	0 Wm^{-2}	80 Wm^{-2}
Warm surface albedo α_W	0.08	0.04
Frozen surface albedo α_C	0.7	0.7
Incident solar radiation Q	173.2 Wm^2	418.8 Wm^{-2}
Tropopause height Z	9 km	17 km

Table 2. Summary of parameters used in the Tropics EBM. Relative humidity δ is higher in the Tropics that the Arctic, and the forcings F_O and F_A are negative instead of positive. The forcing F_C is explained in the text. The insolation Q is as determined by McGeehee and Lehman (2012). Tropopause height Z is from Kishore et al. (2006). Parameters not listed here are the same as for the Arctic, see Table 1.

15   The new entry in this Table, one that did not appear in the polar models, is F_C, which represents transport of heat away from the surface to the atmosphere, by conduction / convection / change of state of water. The most important of these is the upward transport of latent heat. Surface water evaporates, taking heat from the surface. As warm moist air rises and cools, the water vapour condenses, releasing its latent heat into the surrounding atmosphere. This transfer is estimated at about $F_C = 80\,\mathrm{Wm}^{-2}$ in the Tropics (IPCC (2013)). In the surface energy balance equation this quantity is negative, while in the Atmosphere equation

its contribution is positive. After normalization, $f_C = \frac{F_C}{\sigma T_R^4}$. With these changes, the EBM (36)(37) becomes, for the Tropics

$$i_A = f_A + f_C + \eta_{CW}(\tau_S) \cdot \tau_S^4, \tag{43}$$

$$i_A = \frac{1}{\beta}\left(\tau_S^4 - [1 - \alpha(\tau_S)]q + f_C - f_O\right). \tag{44}$$

Figure 8 a) shows solutions of these EBM equations for Tropical parameter values. Note that at no value of the forcings used here does the warm equilibrium point approach a saddlenode bifurcation point. Thus, our EBM is in agreement with the geological record.
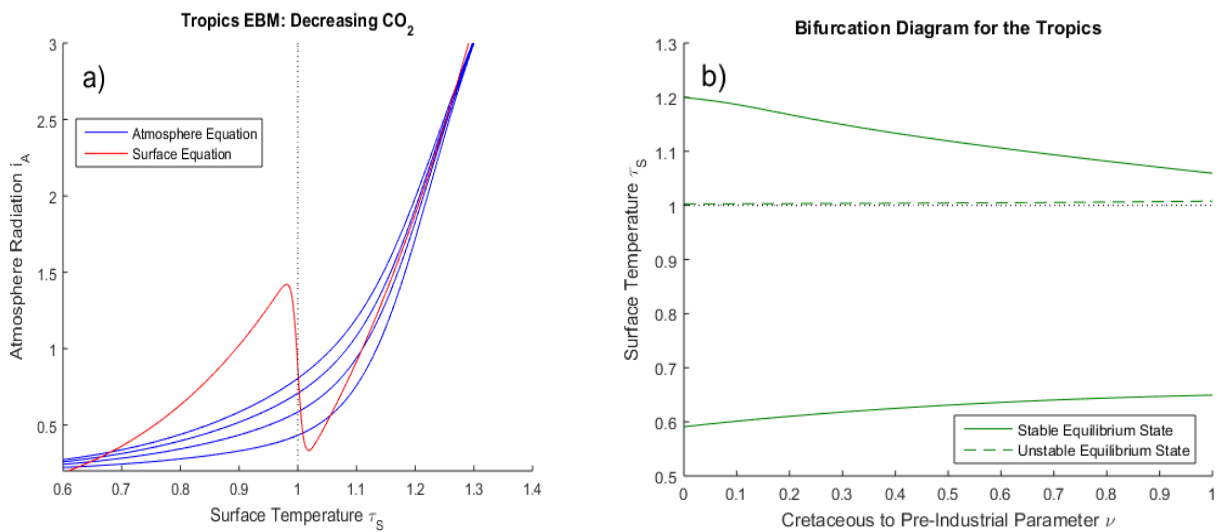
Figure 8. Tropics EBM, using equations (43)(44) and parameter values as in Table 2. Subfigure a): The blue curves represent the atmosphere equilibrium equation for $\mu = 1200, 900, 600, 300$, from top to bottom. Subfigure b): Bifurcation Diagram for the Tropics EBM. Here, CO_2 concentration μ and ocean heat transport F_O are both decreasing, with increasing ν, $(0 \leq \nu \leq 1)$, as given by equations (45). As ν varies, both the warm equilibrium state ($\tau_S > 1$) and the frozen equilibrium state ($\tau_S < 1$) persist; there are no saddlenode bifurcations.

A bifurcation diagram is constructed for the Tropics EBM, spanning mid-Cretaceous to modern pre-industrial times, similar to those for the Antarctic and Arctic glaciations. Here $\nu = 0$ corresponds to mid-Cretaceous values and $\nu = 1$ corresponds to modern pre-industrial values. We let μ and F_O decrease linearly with ν.

$$\mu = 1130 - 860 \cdot \nu \tag{45}$$

$$F_O = -55 + 29 \cdot \nu.$$

The mid-Cretaceous CO_2 concentration $\mu = 1130$ is as determined by Fletcher et al. (2008), see Table 3. The ocean heat transport $F_O = -55$, from the Tropics in the mid-Cretaceous, is from Barron et al. (1981). Astrophysicists have determined that solar luminosity is slowly increasing with time (Sagan and Mullen (1972)). For the mid-Cretaceous, insolation was approximately 1% less than it is today (Barron (1983)). This difference is considered too small to be significant in our model.

The bifurcation diagram for the Tropics EBM is shown in Figure 8 b). Note that no bifurcations occur for parameter values relevant to the Tropics. This is in agreement with paleoclimate records that show little change in Tropical climate, even when polar climates change dramatically.

3.4 EBM for the Warm Equable Cretaceous Problem

One hundred million years ago, in the mid-Cretaceous period, the climate of Earth was much more *equable* than today. "More equable" means that the pole-to-equator temperature gradient was much smaller, and also the seasonal summer/winter temperature variations were much smaller. The climate in the Tropics was only slightly warmer than today, but the climate at both poles was much warmer than today. An abundance of plant and animal life thrived under these conditions, from the equator to both poles, including of course dinosaurs. The question of how this globally ice-free climate could have been maintained has been called a fundamental problem in paleoclimatology (Barron et al. (1981); Barron (1983); Cronin (2010)).

There have been many attempts to explain this difference in climate (Bice et al. (2006); Barron et al. (1981, 1995); Barron (1983); Cronin (2010); Pagani et al. (2005); Ruddiman, Ch. 6 (2014); Sloan and Barron (1992)). General Circulation Models (GCM) adjusted to mid-Cretaceous forcing parameter values have failed to give good agreement with climate proxies. In order to obtain polar temperatures in agreement with mid-Cretaceous values, these simulations typically have assumed increased CO_2 levels more than 4 times modern levels; but then the tropical temperatures predicted by the models were too high. Barron (1983) called this the *warm, equable Cretaceous climate problem*. Later, Sloan and Barron (1990) speculated that continental interiors had cold winters even in the Cretaceous; however, that proposal has been challenged (Wing and Greenwood (1993)). Based on ocean drilling samples, Bice et al. (2006) estimate Cretaceous CO_2 concentrations between 600 ppmv and 2400 ppmv, and tropical Atlantic upper ocean temperatures between $33°C$ and $42°C$. Based on fossil samples, Fletcher et al. (2008) estimate mid-Cretaceous atmospheric CO_2 concentrations of 1130 ppmv and we choose their estimate for use in this EBM, see Table 3.

Forcing Parameters for the mid-Cretaceous EBM, 100 Ma		
Parameter	**mid-Cretaceous Value**	**Source**
CO_2 level μ	1130 ppm	Fletcher et al. (2008)
Relative humidity δ	0.67	Jahren and Sternberg (2003)
Antarctic ocean heat transport F_O	100 W m^{-2}	Barron et al. (1981)
Arctic ocean heat transport F_O	60 W m^{-2}	Barron et al. (1981)
Atmospheric heat transport F_A	41 W m^{-2}	Barron et al. (1981)

Table 3. Summary of parameters used in the Polar Cretaceous model. The main difference in Cretaceous climate between the two poles was that ocean heat transport was much higher in the Antarctic. Parameters not listed here are the same as for today's Arctic, see Table 1. The value of F_A shown here is an average of estimates in Barron et al. (1981).
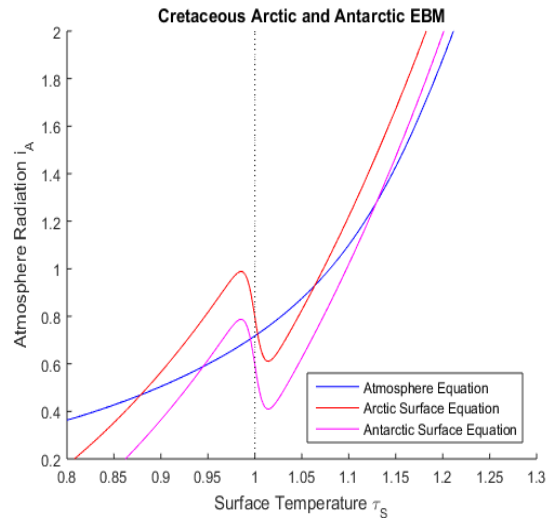
Figure 9. Solutions of the mid-Cretaceous EBM for both poles, using parameter values in Table 3. The blue curve represents the atmosphere equilibrium equation, which is the same for both poles. The two Z-shaped curves represent the Arctic (upper orange curve) and the Antarctic (lower magenta curve) surface equilibrium equations. The only difference in these two is that ocean heat transport F_O is much greater in the Antarctic than the Arctic. Both poles support both warm and frozen equilibrium states. (This figure is referenced also in Section 3.5.)

Paleoclimate data from the mid-Cretaceous show little difference in climate between the two warm poles at that time. However, major changes in climate have taken place since that time, at both poles. The major difference in forcings between the two poles at that time was that ocean heat transport F_O was much higher in the Antarctic than the Arctic, as shown in

5   Table 3. This is due to the location of the South Pole in open ocean during the Cretaceous, as the continent of Antarctica had not yet drifted to its present position over the South Pole. Therefore, we model the mid-Cretaceous climate at the two poles using equations (36)(37), with two values of F_O as in Table 3, and all other forcings the same for the Arctic and Antarctic.

The EBM equilibrium curves are shown in Figure 9, where it is clear that a warm ($\tau_S > 0$) equilibrium state exists at both poles, for the given parameter values. The Antarctic equilibrium state is the warmer of the two, because of the higher ocean

10   heat transport F_O to the Antarctic. From Section 3.3, the Tropical region of Earth also had a warm equilibrium state under mid-Cretaceous conditions. Therefore, the EBM of this paper implies existence of a pole-to-pole, warm, equable Cretaceous climate, as is seen in the geological record.

Figure 9 also implies that a frozen equilibrium state is mathematically possible at each pole during the Cretaceous. In that case, the Tropics could remain in its warm state, thus giving the mathematical possibility of a Cretaceous climate that is

15   *not equable*, but has warm Tropics and ice-covered poles, like today's climate. This may help explain why some computer simulations, starting from today's climate conditions, found a Cretaceous climate that resembled today's climate, rather than the warm, equable climate that actually existed in the Cretaceous.

3.5 EBM for the Eocene Equable Climate Problem

The climate of the early Eocene Epoch (≈ 50 million years ago) was the warmest of the past 65 million years, but a little cooler than the Cretaceous, see Cronin (2010); Pagani et al. (2005); Sloan and Barron (1992); Sloan and Rea (1995). Both poles were

5 ice-free and the pole to equator temperature gradient was much smaller than today. Computer simulations, based on modern climate conditions, have failed to reproduce the early Eocene warm equable climate, see Huber and Caballero (2011); Jahren and Sternberg (2003); Sloan and Barron (1990, 1992). This discrepancy has been called the *Eocene equable climate problem*.

The main difference in forcings between early Eocene conditions and those of the mid-Cretaceous, is that the global CO_2 concentration μ may have been a little lower and the ocean heat transport F_O to the Antarctic was less. Referring to Figure 9,

10 this means that the blue atmosphere equilibrium curve moves downward slightly and the magenta Antarctic surface equilibrium curve moves upward. The orange Arctic surface equilibrium curve does not change significantly. With these small changes, all of the equilibrium climate states (intersection points) persist in Figure 9. Therefore, adaptation of the EBM of this paper to early Eocene climate conditions yields results very similar to those of Section 3.4 for the mid-Cretaceous climate. The figure for the Eocene EBM (not shown here) is topologically the same as Figure 9 for the mid-Cretaceous EBM,

15 Thus, the EBM predicts that a warm (ice-free) equilibrium state exists (mathematically) at both poles in the Eocene. From Section 3.3, the equatorial region also has a warm equilibrium state for Eocene conditions. Therefore, this EBM study supports the existence of a pole-to-pole, warm, equable climate in the Eocene Epoch.

4 Conclusions and Future Work

This paper presents a new energy balance model (EBM) for the climate of Earth, one that elucidates the distinctive roles of

20 carbon dioxide and water vapour as greenhouse gases, and also the role of ice-albedo feedback, in climate change. Nonlinearity of the EBM leads to multiple solutions of the mathematical equations and to bifurcations that represent transitions between coexisting stable equilibrium states. This EBM sheds new light on several important problems of paleoclimate science; namely, the glaciation of Antarctica, the Pliocene Paradox, the warm equable mid-Cretaceous climate problem and the warm equable early Eocene climate problem. Predictions of the EBM are in qualitative agreement with the paleoclimate record.

25 Some readers may challenge the choices of paleoclimate parameter values used in this paper. There has been a wide range of values published in the paleoclimate literature, in particular for mid-Cretaceous and Eocene CO_2 concentrations and temperatures. The specific choices made here, while informed by proxies, are somewhat arbitrary. However, this fact does not affect the validity of our main conclusions. The *coexistence of multiple solutions* and the *bifurcations* demonstrated in the EBM, are robust phenomena. That is, the existence of these multiple solutions and bifurcations will persist, over a range of values of

30 the forcing parameters. The main conclusion of this paper, that sudden and significant changes in climate have occurred, even while forcing parameters were changing very gradually, follows from the existence of mathematical bifurcations in the EBM, not from particular choices of the forcing parameters.

As the paleoclimate record becomes clearer, there is growing evidence for relatively rapid fluctuations in some parameter values, including CO_2 concentrations, over the geological time period studied here; see Cronin (2010); Pagani et al. (1999,

2005). The model of this paper assumes a smooth decline in CO_2 concentration. However, this does not invalidate our main conclusions. The theory of Stochastic Bifurcation (Namachchivaya (1990); Arnold et al. (1996)) tells us that, if stochastic noise is added to a deterministic bifurcation problem, the location of the bifurcation (in terms of the bifurcation parameter)

5 may change, but the *existence* of the bifurcation is preserved.

Further work on this EBM is in progress. Having demonstrated the validity of the EBM on known paleoclimate transitions, this EBM is now being applied to anthropogenic climate change, with the goal of predicting the climate effects of continued increases in CO_2 concentration, now and in future centuries. Next, this scalar EBM will be generalized to a two-point boundary value problem in the altitude variable z, using the Schwarzschild equations to replace the ICAO International Standard

10 Atmosphere approximation. That change will more accurately model the behaviour of the greenhouse gases. Next, the one-dimensional EBM BVP will be incorporated into a generalization of the spherical shell PDE model of Lewis and Langford (2008); Langford and Lewis (2009). This zonally symmetric Navier-Stokes Boussinesq system will enable the study of a third positive feedback mechanism (in addition to the two studied in this paper); namely, Hadley cell convection feedback, which influences atmospheric heat transport F_A. Hadley cell feedback appears to have played a role in the warm equable Cretaceous

15 climate problem, and it may be enhancing the effects of anthropogenic forcing in climate change today.

Code availability. The original Matlab code for the computations that support this research is available in the Appendix of: Dortmans (2017).

Author contributions. W.F. Langford contributed the original hypothesis on which the investigation is based, guided the work, and wrote most of this final paper. B. Dortmans carried out the computations required for this research and wrote a thesis on his work, which was the starting point for this paper. A.R. Willms co-supervised B. Dortmans' work and contributed insights for this paper.

20 *Competing interests.* The authors declare that they have no conflict of interest.

Acknowledgements. The authors acknowledge financial support of this work by the Natural Sciences and Engineering Research Council of Canada. W.F. Langford gratefully acknowledges very helpful discussions with J.F. Basinger and D.R. Greenwood.

References

Arnold, L., Namachchivaya, N. Sri and Schenk, K. Toward an understanding of stochastic bifurcation: Case study. Internat. J. Bifur. Chaos 6, (1996) 1947–1979.

5   Ballantyne, A.P., Greenwood, D.R., Sinninghe Damsté, J.S., Csank, A.Z., Eberle, J.J., and Rybczynski, N. Significantly warmer Arctic surface temperatures during the Pliocene indicated by multiple independent proxies. Geology 38, (2010) 603–606.

Barron, E.J., Thompson, S.L. and Schneider, S.H. An ice-free Cretaceous? Results from climate model simulations. Science 212, (1981) 10–13.

Barron, E.J. A warm, equable Cretaceous: the nature of the problem. Earth-Sci. Rev., 19, (1983) 305–338.

10   Barron, E.J., Fawcett, P.J., Peterson, W.H., Pollard, D. and Thompson, S.L. A "simulation" of mid-Cretaceous climate. Paleoceanography 10, (1995) 953–962.

Bartoli, G., Sarnthein, M., Weinelt, M., Erlenkeuser, H., Garbe-Schönberg, D. and Lea, D.W. Final closure of Panama and the onset of northern hemisphere glaciation. Earth Plan. Sci. Lett. 237, (2005) 33–44.

Basinger, J.F., Greenwood, D.R. and Sweda, T. Early Tertiary vegetation of Arctic Canada and its relevance to Paleoclimatic interpretation. In:
15   M.C. Boulter and H.C. Fisher, Cenozoic Plants and Climate of the Arctic. NATO ASI Series, Vol. 127, (1994) 175–198, Springer-Verlag.

Bice, K.L., Birgel, D., Meyers, P.A., Dahl, K.A., Hinrichs, K-U., and Norris, R.D. A multiple proxy and model study of Cretaceous upper ocean temperatures and atmospheric CO_2 concentrations. Paleoceanography, 21, (2006). doi:10.1029/2005PA001203

Briggs, J.C. Biogeography and Plate Tectonics. Elsevier, Amsterdam (1987).

Budyko, M.I. The effect of solar radiation variations on the climate of the Earth. Tellus XXI 5, 611–619 (1968).

20   Cronin, T.M. Paleoclimates: Understanding Climate Change Past and Present. Columbia University Press, New York (2010).

Csank, A.z., Patterson, W.P., Eglington, B.M., Rybczynski, N., Basinger, J.F. Climate variability in the Early Pliocene Arctic: annually resolved evidence from stable isotope values of sub-fossil wood, Ellesmere Island, Canada. Pal. Pal. Pal. 398, (2011) 339–349.

DeConto, R.M., Pollard, D., Wilson, P.A., Pälike, H., Lear, C.H. and Pagani, M. Thresholds for Cenozoic bipolar glaciation. Nature 455, (2008) 652–657.

25   Dortmans, B. A Conceptual Model of Climate Change Incorporating the Roles of Carbon Dioxide and Water Vapour as Greenhouse Gases. M.Sc. Thesis, Department of Mathematics and Statistics, University of Guelph (2017)

Dortmans, B., Langford, W.F. and Willms, A.R. A conceptual model for the Pliocene paradox. Department of Mathematics and Statistics, University of Guelph, Submitted for publication (2017).

Fedorov, A. V., Dekens, P. S., McCarthy, M., Ravelo, A. C., deMenocal, P. B., Barreiro, M., Pacanowski, R. C. and Philander, S. G. The
30   Pliocene paradox (Mechanisms for a permanent El Niño). Science 312, (2006) 1485–1489.

Fedorov, A.V., Brierley, C.M. and Emanuel, K. Tropical cyclones and permanent El Niño in the early Pliocene epoch. Nature 463, (2010) 1066–1070.

Fletcher, B.J., Brentnall, S. J., Anderson, C. W., Berner, R. A. and Beerling, D. J. Atmospheric carbon dioxide linked with Mesozoic and early Cenozoic climate change. Nature Geoscience 1, (2008) 43–48.

35   Fretwell, P., Pritchard, H. D., Vaughan, D. G., Bamber J. L., Barrand, N. E., Bell, R., Bianchi, C., Bingham, R. G., Blankenship, D. D., Casassa, G., Catania, G., Callens, D., Conway, H., Cook, A. J., Corr, H. F. J., Damaske, D., Damm, V., Ferraccioli, F., Forsberg, R., Fujita, S., Gim, Y., Gogineni, P., Griggs, J. A., Hindmarsh,R. C. A., Holmlund, P. J., Holt, W., Jacobel, R. W., Jenkins, A., Jokat, W., Jordan, T., King, E. C., Kohler, J., Krabill, W., Riger-Kusk, M., Langley, K. A., Leitchenkov, G., Leuschen, C., Luyendyk, B. P., Matsuoka, K.,

Mouginot, J., Nitsche, F. O., Nogi, Y., Nost, O. A., Popov, S. V., Rignot2, E., Rippin, D. M., Rivera, A., Roberts, J., Ross, N., Siegert, M. J., Smith, A. M., Steinhage, D., Studinger, M., Sun, B.,Tinto, B. K., Welch, B. C., Wilson, D., Young, D. A., Xiangbin, C., and Zirizzotti, A. Bedmap2: improved ice bed, surface and thickness datasets for Antarctica. Cryosphere 7, (2013) 375–393.

5 Goldner, A., Herold, N. and Huber, M. Antarctic glaciation caused ocean circulation changes at the Eocene?Oligocene transition. Nature 511, (2014) 574–577.

Greenwood, D. R., Basinger, J. F. and Smith, R. Y. How wet was the Arctic Eocene rain forest? Estimates of precipitation from Paleogene Arctic macrofloras. Geology 38, (2010) 15–18.

Haug, G.H., Tiedemann, R. and Keigwin, L.D. How the Isthmus of Panama put ice in the Arctic. Oceanus 42, (2004) 1–4.

10 Huber, M. and Caballero R. The early Eocene equable climate problem revisited. Clim. Past 7, (2011) 603–633.

Intergovernmental Panel on Climate Change. Climate Change 2013: The Physical Science Basis. Contribution of Working Group I to the Fifth Assessment Report of the Intergovernmental Panel on Climate Change. [Stocker, T.F., D. Qin, G.-K. Plattner, M. Tignor, S.K. Allen, J. Boschung, A. Nauels, Y. Xia, V. Bex and P.M. Midgley (eds.)]. Cambridge University Press, Cambridge, United Kingdom and New York, NY, USA, (2013) 1535 pp. [Also available at http://www.ipcc.ch/]

15 International Civil Aviation Organization. Manual of the ICAO Standard Atmosphere: extended to 80 kilometres. Third Edition. ICAO, 1000 Sherbrooke Street West Suite 400, Montreal, Quebec, Canada H3A 2R2 (1993)

Jahren, A.H., and Sternberg, L.S.L., Humidity estimate for the middle Eocene Arctic rain forest. Geology 31, (2003) 463–466.

Kaper, H. and Engler, H. Mathematics and Climate. Society for Industrial and Applied Mathematics, Philadelphia USA (2013)

Kishore, P., Namboothiri, S.P., Igarashi, K., Jiang, Jonathan H., Ao, Chi O., and Romans, Larry J. Climatological characteris-
20 tics of the tropopause parameters derived from GPS/CHAMP and GPS/SAC-C measurements. J. Geophys. Res., 111, (2006) doi:10.1029/2005JD006827

Kuznetsov, Y.A. Elements of Applied Bifurcation Theory. Third Edition. Springer, New York, (2004).

Langford, W.F. and Lewis, G.M. Poleward expansion of Hadley cells. Can. Appl. Math. Quart. 17, (2009) 105–119.

Lewis, G.M. and Langford, W.F. Hysteresis in a rotating differentially heated spherical shell of Boussinesq fluid. SIAM J. Appl. Dyn. Syst.
25 7, (2008) 1421–1444.

McGehee, R. and Lehman, C. A paleoclimate model of ice-albedo feedback forced by variations in Earth's orbit. SIAM J. Appl. Dynam. Sys. 11, (2012) 684–707.

Namachchivaya, N. Sri. Stochastic Bifurcations. J. Appl. Math. Comput., 38, (1990) 101–159.

North, G.R., Cahalan, R.F. and Coakley, J.A. Energy balance climate models. Rev. Geophys. Space Phys. 19, (1981) 91–121.

30 Pagani, M., Arthur, M. A. and Freeman K. H. Miocene evolution of atmospheric carbon dioxide. Paleoceanography 14, (1999) 273–292.

Pagani, M., Caldeira, K., Archer, D. and Zachos, K. C.. An ancient carbon mystery. Science 314, (2006) 1556–1557.

Pagani, M., Huber, M., Liu, Z., Bohaty, S.M., Henderiks, J., Sijp, W., Krishnan, S. and DeConto, R.N. The role of carbon dioxide during the onset of Antarctic glaciation. Science 334, (2011) 1261–1264.

Pagani, M., Zachos, J.C., Freeman, K.H., Tipple, B. and Bohaty, S. Marked decline in atmospheric carbon dioxide concentrations during the
35 Paleogene. Science 309, (2005) 600–603.

Payne, A. E., Jansen, M. F. and Cronin, T. W. Conceptual model analysis of the influence of temperature feedbacks on polar amplification. Geophys. Res. Lett. 42, (2015) 9561–9570.

Pierrehumbert, R.T. Principles of Planetary Climate. Cambridge University Press, Cambridge UK (2010)

Ruddiman, W.F. Earth's Climate Past and Future. Third Edition. W.H. Freeman and Company (2014)

Sagan, C. and Mullen, G. Earth and Mars: Evolution of atmospheres and surface temperatures. Science, New Series, 177, (1972) 52–56.

Scher, H.D., Whittaker, J.M., Williams, S.E., Latimer, J.C., Kordesch, W.E.C. and Delaney, M.L. Onset of Antarctic Circumpolar Current 30 million years ago as Tasmanian Gateway aligned with westerlies. Nature 523, (2015) 580–583.

5 Sellers, W. D. A global climate model based on the energy balance of the earth-atmosphere system. J. Appl. Meteo. 8, (1969) 392–400.

Sloan, S. B. and Barron, E. J. "Equable" climates during Earth history? Geology 18, (1990) 489–492.

Sloan, S. B. and Barron, E. J. A comparison of Eocene climate model results to quantified paleoclimatic interpretations. Pal. Pal. Pal. 93, (1992) 183–202.

Sloan, S. B. and Rea, D. K. Atmospheric carbon dioxide and early Eocene climate: A general circulation modeling sensitivity study. Pal. Pal.
10 Pal. 119, (1995) 275–292.

Struzik, E. Future Arctic: Field Notes from a World on the Edge. Island Press, Washington, DC (2015)

Tedford, R.H. and Harington, C.R. An Arctic mammal fauna from the Early Pliocene of North America. Nature 425, (2003) 388–390.

Watanabe, T., Suzuki, A., Minobe, S., Kawashima, T., Kameo, K., Minoshima, K., Aguilar, Y.M., Wani, R., Kawahata, H., Sowa, K., Nagai, T. and Kase T. Permanent El Niño during the Pliocene warm period not supported by coral evidence. Nature 471, (2011) 209–211.

15 West, C.K., Greenwood, D.R. and Basinger, J.F. Was the Arctic Eocene 'rainforest' monsoonal? Estimates of seasonal precipitation from early Eocene megafloras from Ellesmere Island, Nunavut. EPSL 427, (2015) 18–30.

Wing, S.L. and Greenwood, D.R. Fossils and fossil climate: the case for equable climate interiors in the Eocene. Phil. Trans. Roy. Soc. B 341, (1993) 243–252.

Wolfe, A. E., Reyes, A.V., Royer, D. L., Greenwood, D. R., Doria, G., Gagen, M. H., Siver, P. A., and Westgate, J. A. Middle Eocene CO2 and climate reconstructed from the sediment fill of a subarctic kimberlite maar. Geology 45, (2017) 619–622.